Study of the Effect of the Geometrical Parameters of the Runner and Operation Conditions on Performance and Flow Characteristics in a Cross Flow Turbine

Juan Diego Peláez Restrepo

Submission date: June 2014
Responsible professor: Luis Santiago Paris L, Universidad Eafit

Universidad Eafit
Department of Mechanical Engineering

Abstract

Keywords: Cross flow turbine, Experimental Tests, Turbine characteristic curves, Design parameters, Turbine efficiency, hydraulic turbine

Due to technological development, massive use of technology, and accelerated population growth in some regions of the planet, the use of renewable energy sources is important to match the increasing electric energy demand.

Hydropower is an important source of renewable energy around the world, due to its simple but efficient way to provide clean electricity generation. Currently, the cross flow turbine also known as Banki-Turbine has been increasingly used in many places around the world due to its simple structure, modest efficiency and its good performance in small and low head hydroelectric applications. It is presumed that the massive utilization of this turbines has been limited due to its low efficiency compared to other turbines with efficiencies near to 90%. Improving this turbine efficiency would make it more attractive and competitive. This can be achieved by means of studying the turbine operation and determining the most significant parameters in its performance. Therefore, the interest of this work is to investigate the performance of the cross flow turbine and the flow characteristics through the turbine.

Two kind of analysis are performed in this work. The objective of the first analysis is to perform experimental tests of some cross flow turbine prototypes under different operating conditions, and determine its performance. Due to the differences in the geometrical parameters of the runner on every prototype, an extensive work of design, manufacture and assemble was required for the execution of the experiments in order to obtain satisfactory results. In the second analysis, CFD simulations of the prototypes are performed with the objective of visualizing the flow through the turbine.

Results show that the turbines with the geometrical parameters selected have a poor performance (approx 50%) under the operating conditions tested. The prototypes with the best performance are those where the nozzle leads the water to a well defined cross flow in the runner, and the water absolute velocity when entering the runner first and second stage corresponds well to the blade angles. The prototypes tested show a disordered flow pattern through the runner with big recirculation zones and poorly correspondence with the water velocity vectors and the blade angles, which increases losses and leads to lower efficiencies.

Contents

List of Figures

List of Tables

Chapter 1

Introduction

Hydro power is in the present the leading renewable energy due to its simple but efficient way to provide clean electricity generation. The major advantage is that water is a source of cheap power, besides, since there is no fuel consumption, the hydroelectric power plants produce less air pollution compared with thermal and nuclear plants. However, the use of water to produce electricity has its limitations, like other energy sources, including environmental impacts caused by damming rivers and streams, which affects the local ecosystem and population. But small hydroelectric plants whose generation power is less than 10MW offer an attractive solution to the power needs of the less-developed countries in the world, because of the abundant energy resources to develop [4].

Small hydroelectric projects have a low environmental impact, which is a crucial issue nowadays. Currently, the cross flow turbine(CFT) also known as Banki-Turbine is used in many places around the world due to its simple structure, modest efficiency (approx 84%) and its good performance in small and low head hydroelectric applications. It is presumed that the massive utilization of this turbines has been limited due to its low efficiency compared to other turbines with efficiencies near to 90%.

The improvement of this turbine efficiency would make it more attractive and competitive, this can only be achieved by means of studying the turbine operation and determining the most significant parameters in its performance. Turbines studied in this project are intended to be used in small hydroelectric applications where the available water flow rate is low, which is the reason why some turbine dimensions are smaller than the dimensions of the turbines studied in other research projects.

1.1.   Objectives

The main objective of this work is to study the effect on performance and flow pattern of the geometrical parameters of the runner, and operation conditions in a cross flow turbine by means of experimental tests and computational fluid dynamics (CFD) simulations. The objective is reached in the following steps:

1. Build some cross flow turbine prototypes with different runner geometrical configurations.

2. Build a test bench with the proper instruments to the measure of variables as pressure, flow rate, torque and rotational speed.

3. Perform some experimental tests of the prototypes under different operation conditions.

4. Determine the performance of each turbine prototype with the data collected in the experimental tests.

5. Develop a design of experiments analysis using the results of experimental tests.

6. Perform some CFD simulations of the turbine prototypes.

7. Evaluate qualitatively the flow pattern through the cross flow turbine prototypes in the CFD simulations results.

This work pretends to contribute in the search for a more efficient cross flow turbine, providing valuable information about the effects of the geometry setup of the runner on the turbine efficiency and its internal flow. It is expected that the results obtained complement the diverse works of other authors. Additionally, this kind of work aids to develop the capability to perform further projects with the purpose of improving the performance of these turbines, so attractive to the nowadays energy demand.

1.2.   Literature Review

This section gives a summary of some of the available literature related with the CFT. The articles described below are divided in three sections, the first one summarize the experimental studies performed on the cross flow turbines, in the second section articles in which CFD studies were conducted are presented. Finally the studies where some modifications were made to the CFT are summarized in the third section.

1.2.1.   Experimental studies

The cross-flow turbine was designed originally in the early twentieth century by the Australian engineer A. G. Michell, and was later studied in the Budapest University by D. Banki between 1917 and 1919. Banki presented in his work the theory of operation of the turbine and experimental results with an efficiency of 80%. Later in 1933, the German engineer Fritz Ossberger designed the cross-flow turbine based on the work of Michell and Banki. Nowadays, the cross-flow turbine is mostly used in small hydroelectric projects located in less developed countries due to its simple design and manufacture.

Compared with other turbines as Pelton or Francis, the cross-flow turbine is not so widely studied. The available research studies have focused mainly in finding the optimum design of the turbine with the use of theoretical and experimental methods.

Previous experimental research about CFT was initiated by Mockmore and Merryfield [5], who studied a turbine made out of steel, with runner side disks of $6.4mm$ thickness and an outer diameter of $332.7mm$. A runner of $305mm$ wide and 20 blades runner were used. The head to test the turbine ranged from $2.74m$ up to $5.49m$, measured to the center of the rotor, with a water flow rate of $0.06m^3/s$ at 4.88m head. A maximum efficiency of 68% was achieved at this point of operation. Mockmore and Merryfield concluded that the maximum efficiency occurs practically at constant speed for all gate openings at constant heads.

Durgin and Fay [6] built a small cross flow turbine where they studied the internal flow characteristics. The investigation revealed that a significant amount of the water did not contribute to second stage energy transfer. The results showed that part of the flow was carried within the runner, and it was concluded that the cross flow did not exist in the form of a very well defined jet. The maximum efficiency obtained was 61% and it was concluded that the second stage contribute the 17% of the power production.

Khosrowpanah [7] studied the performance of the cross-flow turbine by varying the number of blades, the runner diameter and nozzle entry arc under flow/head variations. The models used were designed for a total head of $1.79m$ and a flow rate of $0.03m^3/s$. A total of 4 turbines were studied, with runner diameters between $15.24cm$ and $30.48cm$. The blade inlet and outlet angles were 30 and 90 degrees with the length along the shaft of $15.24cm$. The number of blades used in the experiments were 20, 15 and 10. Nozzles for all the runners had the same length as the blades but varying entry arcs of 58, 78, and 90 degrees. For the four models studied, Khosrowpanah concluded that the maximum efficiency (80%) of the CFT at any flow/head combination increases by increasing the nozzle entry arc from 58 to 90 degrees, and efficiency of the CFT showed strong dependence on the number of blades, the optimum number of blades in his experiment was approximately 15 for the $30.48cm$ runner.

Fiuzat and Akerkar [8] investigated the contribution of the two stages of power generation to the shaft power in a cross-flow turbine. In the experimental procedure the following quantities were measured: flow rate into the turbine, diverted flow, torque at turbine shaft, runner rotational speed and pressure at the nozzle inlet. The investigation concluded that the contribution of the second stage to the total shaft power of the CFT is at least 45% for a nozzle with a 90° entry arc, and at least 41% for a nozzle with an entry arc of 120°.

Joshi, Seshadri and Singh [9] conducted a study with the purpose of evaluating the performance of the turbine for medium and low heads by systematically varying the number of blades from 8 to 30 and the nozzle entry arc from 23° to 36°. The runner had a width of $0.325m$, diameter of $0.3m$ and 20 blades. They concluded that the performance of the turbine improves with an increase in nozzle entry arc, and by increasing the number of blades up to a limit, beyond which it deteriorates. For the turbine studied, the optimum number of blades was 20 approximately.

Venkappayya and Nadim [10] made an experimental investigation to study the effect of some geometric parameters on the efficiency of the cross-flow turbine. The turbine models studied were constructed with three different number of blades between 15 and 25, three different inner to outer radios diameter relation between 0.60 and 0.75, and three different angles of water entry to the runner between 24° and 32°. The conclusions of this study showed that the efficiency increased with increase in the number of blades. However, the increase in the angle of attack did not increase the turbine efficiency in the range of 24 to 32 degrees. The maximum efficiency reached in this study was 84.5%.

Olgun [11] conducted an experimental study to investigate the effects of some geometrical parameters like diameter ratio and throat width ratio, on the efficiency of the cross-flow turbine. Olgun studied four different types of runners, each of these had 28 blades. The blade inlet and outlet angles were 30° and 90°, the inner to outer diameter ratios of runners vary from 0.54 to 0.75. Each runner was tested with two different nozzles, one of the nozzle had an opening angle of 49° and the opening angle of the second nozzle was 104°, additionally the second nozzle had a guide vane in its interior. The efficiency study was developed changing head range from 8 to 30 m, and the highest efficiency obtained was 72%.

Costa Pereira and Borges [12] performed an investigation of the flow inside the nozzle of a CFT. The study consisted in the experimental test of two different nozzles, one with and one without an inside guide vane. The static pressure in the walls of the nozzles was measured by placing 21 pressure tapping, the investigation also included the measurement of the pressure distribution with a rotor assembled in the turbine, as well as the measurement of the turbine. The results showed that the pressure distribution is unaffected by the head. Instead the presence of a rotor affected significantly the pressure inside the nozzle.

Study	Year	Max. Efficiency
Mockmore and Merryfield [5]	1949	68%
Durgin and Fay [6]	1984	61%
Khosrowpanah et al. [7]	1988	80%
Fiuzat and Akerkar [8]	1991	78.8%
Seshadri et al [9]	1995	70% Approx
Venkappayya et al. [10]	1994	84.5%
Olgun [11]	1998	72%
Costa and Borges [12]	1996	54.5%
Walseth [13]	2009	77.5%

Table 1.1: Experimental Studies Summary

Walseth [13] studied the flow pattern through the runner of a cross-flow turbine, in the investigation were performed two different types of experiments. The objective of the first experiment was to visualize the flow through the runner. The second experiment measured the torque transfer to the runner using strain gages installed on the blades. The results showed that the turbine had better performance for large nozzle openings, and in the best operation point the second stage provided the 53.7% of the energy transfered from the water.

A short summary of the experimental works cited above are listed in the table 1.1 with its year of publication and efficiency obtained.

1.2.2. CFD studies

Some investigations of the design parameters and its effects in the performance of the cross flow turbine using numerical and CFD analysis were found.

Fukutomi, Nakase and Watanabe [14] calculated numerically the flow from a nozzle with an arbitrary geometry, the effects of nozzle shape in the flow conditions were also studied. The results showed that the pressure at the outlet of the nozzle has a different value from atmospheric, the results fitted well with experimental data.

Choi et al [15] performed an study that pretended to optimize the structure of cross-flow turbine and to improve its performance using a CFD commercial code. The results of the study showed that the inlet and outlet angles of the runner blades affected considerably the performance of the turbine. It was also possible to determine the hydraulic losses due to the

recirculating flow in the runner.

Choi et al [16] studied the influence of the nozzle shape on the performance of a direct drive turbine for wave energy converter, this turbine has the same geometrical configuration of the cross flow turbine. Four different nozzles were tested numerically using a CFD commercial code. A maximum efficiency of 78% was obtained.

Son et al [17] conducted an investigation in which it was studied the effect of inlet nozzle shape on the performance of a cross-flow turbine for small hydro power by CFD analysis, besides the effect of the shape of draft tube was also studied. Two kinds of inlet nozzle shapes were used in the development of the investigation. The results obtained showed that narrow inlet nozzle shape gaves better effect on the performance of the turbine, moreover the length and the diffuse angle of the draft tube in the turbine model did not influence considerable on the turbine performance.

Choi, Lim, Kim and Lee [18] studied the effect of the turbine's structural configuration on the performance and internal flow characteristics of the cross-flow turbine using CFD analysis. In this study, the following geometrical parameters were varied: the inlet angle to the blade, the outlet angle from the blade, the number of blades and the shape of the nozzle. The results show that these parameters were closely related to the performance of the turbine. The largest effects on the turbine performance were related to the nozzle shape; a narrow nozzle passage resulted in a high turbine efficiency.

Choi et al [19] made a CFD study and field tests experiments in which analyzed the effects in the performance of the air layer in the runner chamber. They suggested also a newly developed air supply method. CFD analysis of the performance and internal flow of the turbine was made with a transient calculation using a two-phase flow model to reproduce the air layer effect on the turbine performance effectively. The turbine model had 30 runner blades, and the inlet and outlet angles of the blade were 30 and 87 degrees, respectively. The widths of nozzle, runner and runner chamber were, b=500mm. The results achieved showed that the air layer in the turbine runner chamber suppressed the recirculation flow in the runner which yielded in a considerable effect on the performance of the turbine.

Marchegiani, Nigro and Storti [20] made a study of the flow in a classical cross flow turbine nozzle using numerical simulations, a model for laminar flow and also a κ-ϵ turbulent model were used in the tests. The results were validated with experimental values.

Chávez and Vera [21] led a CFD analysis using the finite element method (FEM), to study the behavior of a 50 kW cross flow turbine. The efficiency, pressure and velocity fields were calculated for different operation conditions. An efficiency of 51.04% was obtained in the investigation.

Akcan et al [22] developed a numerical study which had as objective the optimization of the structural stress levels for different operation conditions. The results yielded the maximum stress and lowest safety factor for critical runner parts for different combinations of design parameters.

Andrade et al [23] led a CFD steady state flow simulation numerical analysis of the velocity and pressure fields of the turbine within the runner and characterized its performance for different runner speeds. A cross flow turbine model with a specific speed of 63 was used as test object.The turbine model had an external diameter of 294 mm and an internal diameter of 200 mm, the number of runner blades was 24, and the inlet and outlet angles of the blade were 16 and 90 degrees, respectively. They concluded that the flow recirculation in the runner inter blade passages and shocks of the internal cross flow caused considerable hydraulic losses, by which the efficiency of the turbine decreases significantly.

Sammartano et al [24] conducted an investigation in which it was proposed a two-step procedure for examining the best geometry and optimal design of cross-flow type machines, taking full advantage of recently expanded computational capabilities. In the test case, a turbine with 35 blades and an attack angle equal to 22° was analyzed with a CFD commercial code obtaining an efficiency of 86%.

The numerical studies and CFD analysis presented before are summarized in table 1.2

Study	Year	Max. Efficiency
Fukutomi et al.	1985	×
Choi et al.	2009	×
Choi et al.	2009	78%
Son et al.	×	×
Choi et al.	2008	×
Choi et al.	2010	×
Marchegiani et al	×	×
Chávez and Vera	×	51.04%
Akcan et al.	2008	×
Andrade et al	2011	×
Sammartano et al.	2013	86%

Table 1.2: CFD Studies Summary

1.2.3.   Studies with modifications to the Cross Flow Turbine

In some studies, modifications have been made to the cross flow turbine main components. The objective of these modifications is to improve the performance of the turbine, results available on the literature are presented below.

Olgun [25] modified the runner of the turbine adding interior guide tubes, which were designed and used to collect and guide the crossing flow towards the second stage of the runner. Three different guide tubes were tested experimentally, the efficiency was determined for different positions of interior tubes and openings of the nozzle. This investigation found that turbine efficiency with the interior guide tube decreased about 5%. The maximum efficiency obtained was 64%.

Kokubu et al [26] investigated experimentally the flow conditions at various operating conditions. To improve the efficiency of the turbine, the guide vane located inside the nozzle was modified with a current plate. The results show that the current plate installed at the concave surface of the guide vane contributes to improve the efficiency, with a maximum efficiency obtained of 80% approx.

Kokubu et al [27] installed an inner guide inside the runner to guard the shaft from the water jet and to adjust the flow direction. The objective of this modification was to improve the performance of the cross flow turbine. The investigation concluded that inner guide deteriorated the performances obtaining a maximum efficiency of 60% approx.

Kokubu et al [28] developed a new kind of micro cross flow turbine called Eco Cross-Flow Hydro Turbine (ECFT), this turbine was proposed to be used at very low specific speed range of hydropower resources, such as very high-head and considerably small-flow rate water resources. Performance and internal flow characteristics were studied with CFD analysis.

The studies in which modifications to the turbine have been made are listed in table 1.3.

Study	Year	Max. Efficiency
Olgun	2000	64%
Kokubu et al.	2013	80%
Kokubu et al.	2012	60%
Kokubu et al.	2011	×

Table 1.3: Studies with modifications to the turbine summary

There is also available literature that describe thoroughly the operating characteristics of the cross flow turbine, and fabrication guidelines, with a complete description of the calculation and dimensioning of each part of the turbine. The models built in this study were built following indications found in the work of OLADE [3], Zia et al [29], Haimerl [30], Breslin [31] and Mockmore [5].

1.3.   Previous work at Eafit University

An experimental study of the performance of a cross flow turbine was made during the first semester of 2012 [1]. The study described the process of building a prototype of cross flow turbine. The prototype was evaluated experimentally under different conditions of flow and mechanical load. For the application of the load and the determination of the delivered torque a brake was used, whose design resembled a Prony brake. Also other variables were measured, such as: flow rate, pressure head at the inlet of the turbine and the rotational speed. From the experimental data, the prototype turbine operation curves were constructed and the best operating conditions were determined. Some characteristics of the prototype tested are described in table 1.4. The operation curves obtained are shown in figure 1.1, it can be found that a maximum power of $240W$ was obtained with an efficiency of 50%.

In the last semester of 2012 an experimental study was made [2], this study performed the design, assembly and laboratory evaluation of a cross flow turbine generator prototype system. In this project was attempted to integrate a prototype power generation system by coupling an electrical generator to the cross flow turbine, modifications were also proposed for a simple prototype construction and maintenance. Some characteristics of the prototype tested are described in table 1.5.

Runner Diameter	Runner width	Output Power
187mm	40mm	1 kW

Table 1.4: Prototype tested in Peláez work [1] Characteristics

Runner Diameter	Runner width	Output Power
150mm	30mm	0.65 kW

Table 1.5: Prototype tested in Llano work [2] Characteristics
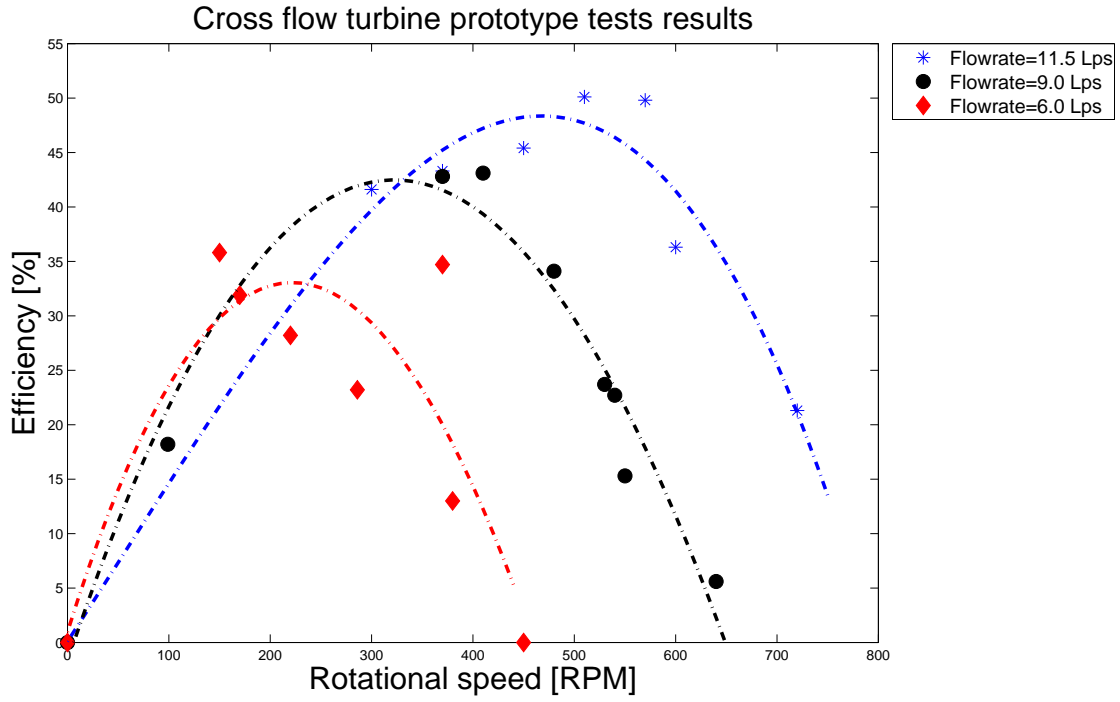
(a) Efficiency Vs. Rotational Speed
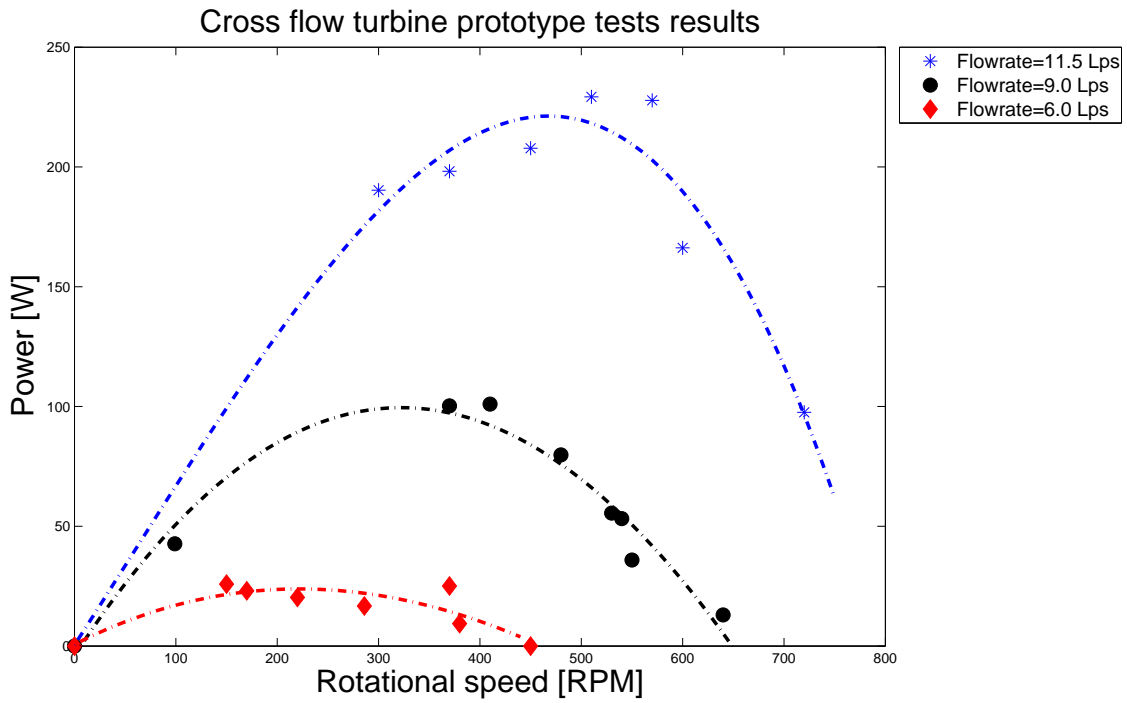
(b) Power Vs. Rotational Speed

Figure 1.1: Operation curves of the prototype tested in Peláez work [1]

Theory

    The cross-flow turbine is a turbine which has as main components a nozzle and a runner. The runner is built up of at least two parallel circular disks fixed by a series of curved blades. The blades are circular and form a certain angle with the inner periphery of the runner (β), this angle defines the path of the water at the outlet of the second stage. The nozzle, whose cross section is rectangular and has a curved back wall, has the main function of directing the flow into the runner at a specific angle of attack (α). This angle is formed by the water absolute velocity and the runner tangential velocity. Figure 2.1 show details of the cross-Flow turbine runner and is used as a sketcth to illustrate the angles mentioned previously.
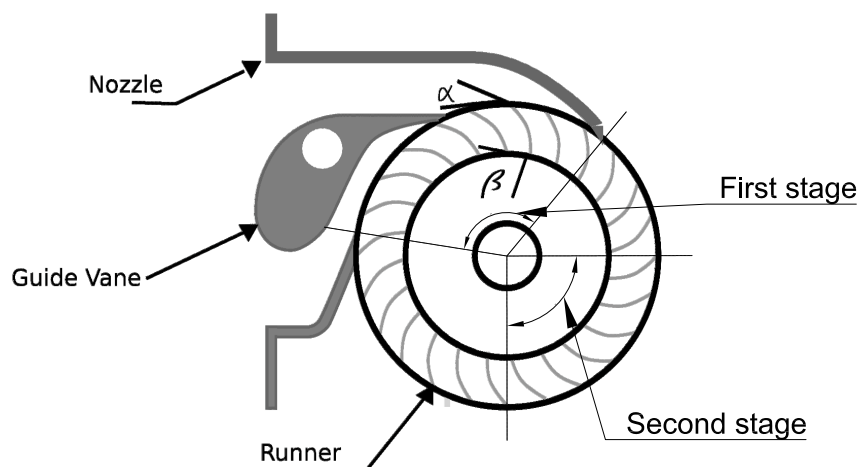
Figure 2.1: Definition sketch of the Cross Flow Turbine

2.1.   Flow description inside a cross flow turbine

The water flows through the nozzle and enters the runner through the nozzle entry arc, the water jet transfers energy to the runner twice, first as it enters the runner and again once it leaves the runner at the opposite side as shown in figure 2.2. A portion of the water that enters the runner nerver reaches the second stage but remains entrained in the runner after entering the first stage, and then leaves the runner [6] [13]. The figure 2.3 shows a description of the cross-flow and the entrained flow mentioned before.
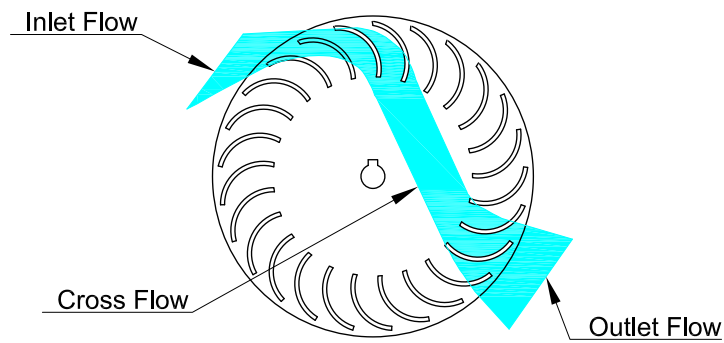
Figure 2.2: Theorical Runner Flow Pattern
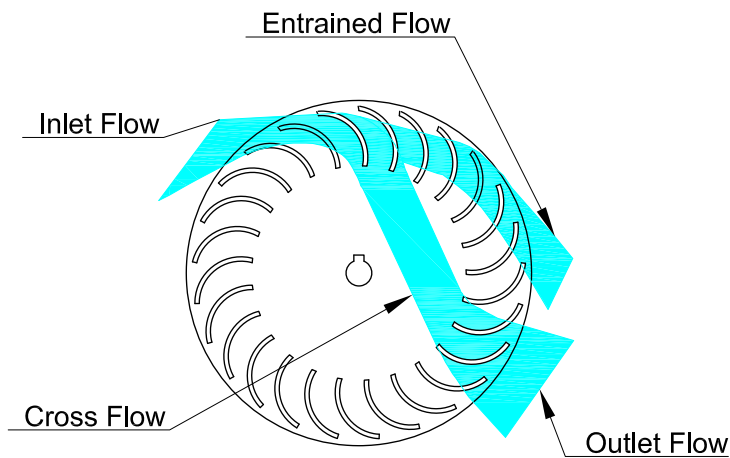
Figure 2.3: Runner with Cross Flow and Entrained Flow Behavior

This turbine is originally classified as an impulse turbine, however, this classification is not strictly correct due to the low positive pressure located at the nozzle outlet and runner inlet. Haimler [30] calculated a pressure rise in the first stage of the turbine equal to 6.3% of the available head, and Walseth [13] found similar characteristics in her experimental study. Although the second stage operates at constant pressure the reaction effect in first stage has led to classify the cross-flow turbine as a borderline turbine.

The cross-flow turbine operating range is defined by the turbine constant $N_{st,US}$, which can be calculated with equation 2.1 or dimensionless version N_{st} which can be calculated as shown in equation 2.2 [32].

$$N_{st,US} = N \frac{P_{out}^{1/2}}{H^{5/4}} \tag{2.1}$$

$$N_{st} = N \frac{P_{out}^{1/2}}{\rho^{1/2}(gH)^{5/4}} \tag{2.2}$$

The table 2.1 shows the cross flow turbine operating range, compared with the operating range of other types of turbines. In the table, it can be seen that the cross flow turbine operating range overlaps the Francis turbine range.

Other turbine constants which affect the turbine performance can be calculated with equations 2.3 and 2.4.

$$Q' = \frac{Q}{D_{int}^2 H^{1/2}} \tag{2.3}$$

$$P' = \frac{P_{out}}{D_{int}^2 H^{5/4}} \tag{2.4}$$

Turbine	$N_{st,US}[\frac{rpmHP^{1/2}}{ft^{5/4}}]$	N_{st}
Pelton	30 - 73	0.69 - 1.67
Cross Flow	60 - 200	1.38 - 4.60
Francis	69 - 450	1.58 - 10.35
Axial	350 - 1000	8.05 - 23.00

Table 2.1: Hydraulic turbines operating range taken from [3]

2.2.   Calculation of the efficiency

The power output of a cross flow turbine can be analyzed by using the Euler turbomachine equation, which expresses that shaft torque is equal to the change in moment of momentum from inlet to outlet of the runner assuming a stationary state and an ideal (viscosity equal to zero) and incompressible (constant density) fluid. The power output of the shaft can be calculated with equation 2.5,

$$W_{shaft} = \omega T_{shaft} \tag{2.5}$$

$\omega \rightarrow$ Shaft rotational speed

$T_{shaft} \rightarrow$ Shaft Torque

where W_{shaft} is given by the Euler turbomachine equation for a turbine, which for a cross flow turbine case is expressed as in equation 2.6.

$$W_{shaft} = \omega T_{shaft} = \rho \omega Q[(C_{1t}r_1 - C_{2t}r_2) + (C_{3t}r_3 - C_{4t}r_4)] \tag{2.6}$$

where C_t represents the tangential component of the water absolute velocity.

$\rho \rightarrow$ Water density

$Q \rightarrow$ Flow Rate

The Euler equation considers the changes in the velocity triangles of the water flowing from runner inlet to outlet of the 1st stage and then from runner inlet to outlet of the 2nd stage. Figure 2.4 shows the velocity triangles for a cross flow turbine. The notation used in this figure is described below.

$U \rightarrow$ Runner Tangential Velocity

$W \rightarrow$ Water Relative Velocity

$C \rightarrow$ Water Absolute Velocity

$r \rightarrow$ Runner radius
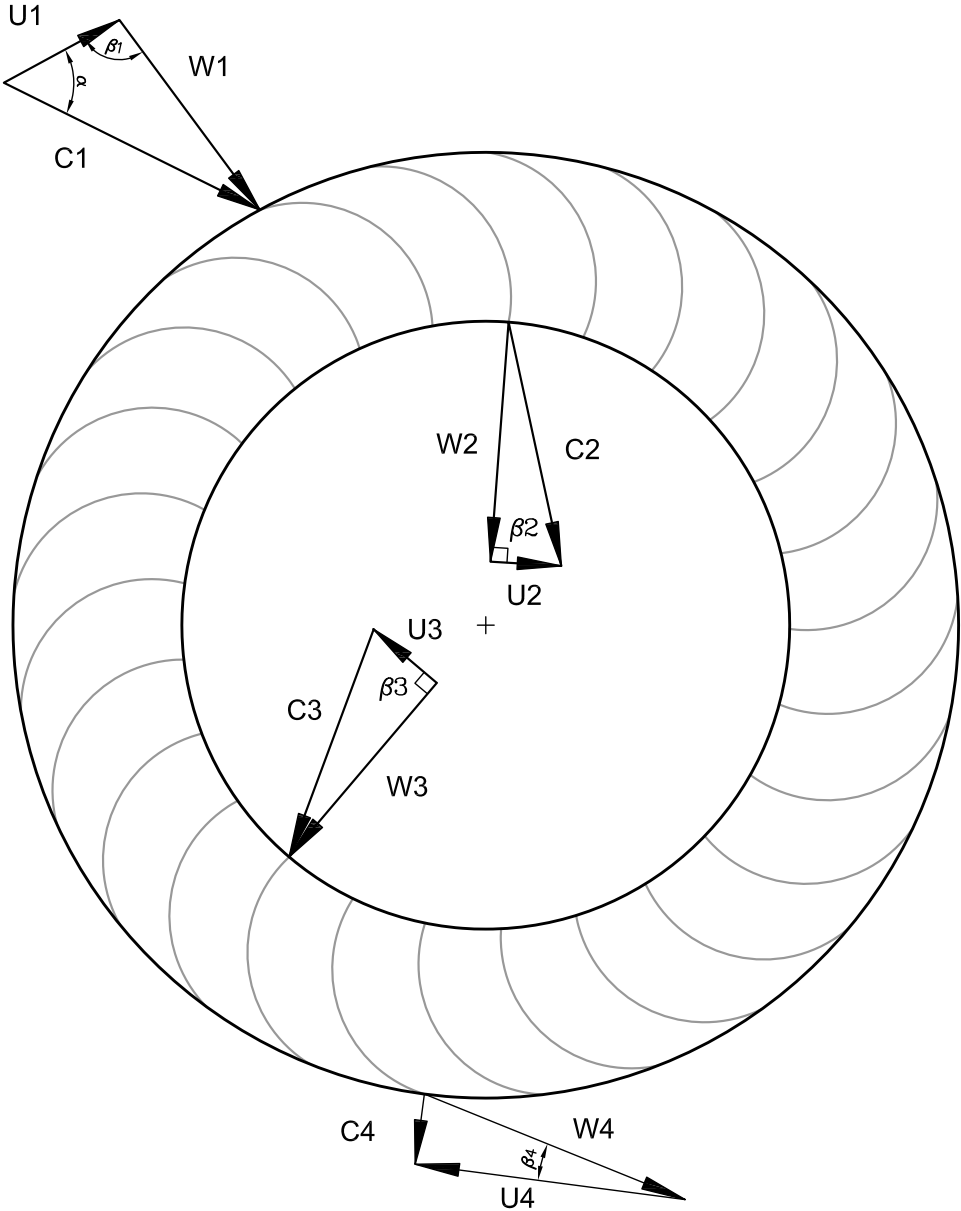
Figure 2.4: Velocity Triangles of a Cross Flow Turbine

Subscript **1** Inlet Stage 1

Subscript **2** Outlet Stage 1

Subscript **3** Inlet Stage 2

Subscript **4** Outlet Stage 2

$\alpha \rightarrow$ Angle between water absolute velocity and runner tangential velocity

$\beta \rightarrow$ Angle between water relative velocity and runner tangential velocity

The hydraulic power can be estimated by using the equation 2.8. where H is the difference between the specific energy head at the turbine inlet and outlet as shown in figure 2.5. The turbine outlet was taken in the water level in the discharge tank. In this point the exit velocity is approximately zero and the pressure is the atmospheric. Therefore, and according to [11] and [33], the net head can be calculated as equation 2.7.

$$H = \frac{P_1}{g\rho} + \frac{V_1^2}{2g} \tag{2.7}$$
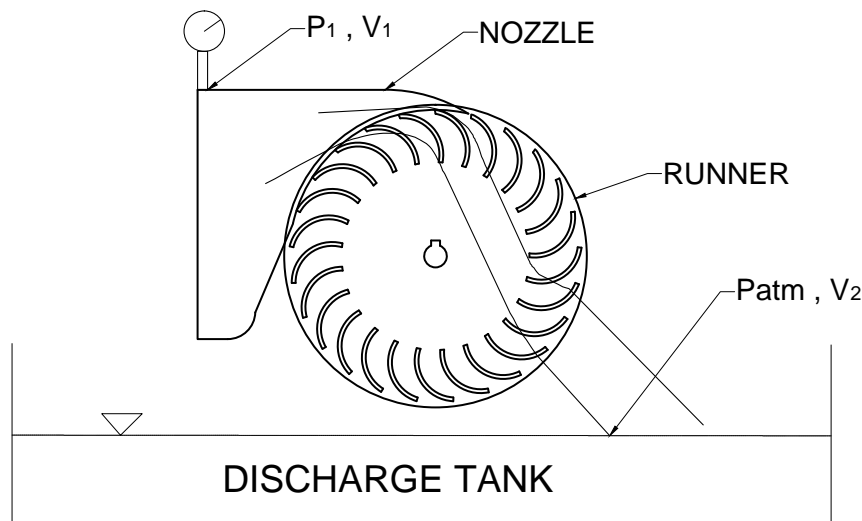
Figure 2.5: Turbine Head

By convention, the turbine efficiency, specifically $\eta_{turbine}$ is defined as the ratio of brake horsepower output (turbine output shaft power) to hydraulic power (power extracted from the water flowing through the turbine), and can be expressed by the equation 2.9.

$$W_{hydraulic} = \rho g Q H \tag{2.8}$$

$\rho \rightarrow$ Water density

$Q \rightarrow$ Flow Rate

$g \rightarrow$ Gravitational Acceleration

$H \rightarrow$ Total Pressure at the Turbine Inlet

$$\eta_{turbine} = \frac{W_{shaft}}{W_{hydraulic}} \tag{2.9}$$

2.3.   Design of Experiments (DOE)

The statistical design of experiments (DOE) is a methodology that allows to obtain enough information, which is statistically analyzed to obtain valuable results, and support the decision making and the understanding of a process [34]. In DOE methodology the experimental tests that must be done and how they will be done, must be defined previously.

DOE method have found broad application in many areas [35]. The experimental process can be an important part of the scientific process, and one of the main ways the people learn about how systems and phenomena work. DOE is then an important tool in the engineering areas in which the performance of many process must be improved constantly. DOE method can be also applied in engineering design activities, where the development of new products an the improvement of the existing ones are performed.

In this work, DOE method was applied to determine the impact of some variables in the performance of the cross flow turbine. The results obtained can be used to identify the variables that most affect the performance and the best operation point of the turbine. The variables studied were geometrical parameters as the number of blades in the runner, the inlet angle to the blade and the outlet angle of the blade, operational parameters were also studied, as the flow rate and the rotational speed.

2.3.1.   Factorial Design

In a factorial design, the objective is to identify the effect of some factors, in one or more answers [34]. A factor can be defined as the process or equipment variables that can be controlled, and it can be both qualitative and quantitative. The effect of a factor is defined as the change in a response produced by a change in the factor. In this kind of experiments, every factor must have, at least, two test levels. A level is the value that can be assigned to every factor studied. In a complete case, there must be tested all the possible combinations that can be formed from the levels of each factor.

2.3.2.   The 2^k Factorial Design

The factorial designs are important because they are widely used in research works [35]. A special case inside the factorial designs is the 2^k factorial design, in this case every factor k takes only two levels, the minimum and the maximum value of a range previously defined. Then the total of possible test combinations, for every factor at every level is 2^k combinations. If the number of factors is greater than 5, is recommended to use a two level fractional factorial design 2^{k-p}, in this case the number of experimental tests are reduced significantly without losing valuable information.

2.4.   Computational Fluid Dynamics (CFD)

Computational Fluid Dynamics (CFD), is a branch of the fluids mechanics, which by means of computer based simulations studies fluid flow, heat transfer, mass transfer, chemical reactions, and related phenomena. CFD is based on numerical methods to solve the mathematical equations which govern these processes that are difficult to solve analytically for general boundary conditions and geometry. In the present the CFD application fields include conceptual designs, detailed product development, troubleshooting, and redesign of systems where fluids are involved.

In experiments, CFD studies provides the opportunity to perform experiments that are very difficult to perform physically, saving a great amount of time and money by replacing material costs, measurement equipment etc. It is also important to understand that the purpose of a CFD study is not to replace the laboratory experiments, it is a complement, and its results must be validated before the model is accepted [36].

2.4.1.   Steps on a CFD Analysis

A CFD analysis has established stages that must be completed to have reliable results. Every study begins with a mathematical model of the physical problem, in which the governing differential equations, boundary conditions and fluid properties must be defined. After that, CFD applies numerical methods to transform the governing equations into a set of algebraic equations and to solve them in a discretized domain. Finally, the solution is post processed to extract quantities of interest. A full list of the CFD analysis steps is described below.

Preprocessing: in this step the geometry, the materials and the discretization (meshing) of the domain are done.

Processing: Solution of the partial differential equations (PDE) using numerical iterative methods for the selected physical model by means of applying mass and moment conservation laws to control volumes within the defined domain.

Postprocessing: In this step the user is able to study the results and make a correct interpretation. In this step is also recommended to make a validation process of the obtained results.

2.4.2.   Governing equations

The governing equations of fluid mechanics that are solved numerically using CFD are mentioned below [37]:

1. Conservation of mass - The continuity equation

$$\frac{\partial \rho}{\partial t} + div(\rho \mathbf{V}) = 0 \tag{2.10}$$

2. Conservation of momentum - The Navier-Stokes equation for an incompressible fluid

$$\rho(\frac{\partial \mathbf{v}}{\partial t} + \mathbf{v} \cdot \nabla \mathbf{v}) = -\nabla p + \rho \mathbf{g} + \mu \nabla^2 \mathbf{v} \tag{2.11}$$

Most hydraulic turbomachinery applications as the cross flow turbine, can be considered isothermal cases, so the conservation of energy equation is not solved for this applications.

2.4.3.   Meshing

In a CFD analysis, the fluid domain is discretized into a finite set of control volumes or cells, for which the different equations are solved. The discretized domain is called the mesh. The importance of meshing process relies upon the quality of the simulation results. The size and type of the mesh elements depend on the problem to be solved and the variables that will be investigated. It is also important to take into account the computational capacity available, since a very refined mesh will require a lot of computational memory and time. The expertise is a very important factor in creating high quality meshes.

2.4.4.   Solver procedures

General conservation (transport) equations for mass and momentum are discretized into algebraic equations to be solved numerically. The solution of these equations can be achieved by different methods, the most popular numerical methods used in CFD simulations are listed below:

1. Finite difference method (FDM): The domain is represented by a set of points and only at those points the results are obtained. The discretization of the equations is performed substituting differential operators with finite differences obtaining an algebraic approximation of the equation. This equation is applied to each point in the domain obtaining a system of algebraic equations.

2. Finite volume method (FVM): The domain is divided in a set of control volumes (CV) and results are obtained at the center of each CV. The system of algebraic equations is obtained by using balance of fluxes in and out of the CV.

3. Finite element method (FEM): The domain is divided in a set of elements where results are obtained at the nodes on the corners or along the edges of the elements. The conservation equation is first expressed using the Method of Weighted Residuals, and dependent variables are approximated by a series of interpolation polynomials (shape functions). Shape functions, multiplied by weight functions, are integrated over each element and these integrals are minimized in order to satisfy the governing equations. The small systems of equations obtained in each element are assembled into a large global system of algebraic equations.

In practical CFD commercial codes, the implementation of the finite volume method is widely used. For the simulation of the CFT prototypes, a research and selection of an adequate

model, as well as good boundary conditions definition is needed. In this work, the selection of the model and physical setup parameters were selected based on studies previously published as [15, 24].

Experimental equipment and procedures

The experimental tests performed had the objective of determining the behavior and performance of four different CFT prototypes. The turbines had runners with different geometrical parameters, but the same nozzle. Every prototype had the same runner width and diameter and was tested under different head conditions and for different runner rotational speed. A statistical design of experiments methodology was also used. The results were used to build the characteristics curves of the turbines, and to identify the variables that most affect the performance of the prototypes.

3.1. Cross flow turbine prototypes

The prototypes were built in the IEXS (spanish acronym for Engineering, Energy, Exergy and Sustainability) research group at Eafit University. The turbines were made of acrylic and consist of a runner, a nozzle and a casing, a 3D model of the turbines is shown in figure 3.1, and some pictures of the constructive process are shown in figure 3.2. A total of four turbines were tested, each prototype had runners with different number of blades, inlet blade angle β_1 and an outlet blade angle β_2. The runner blades number ranges from 15 to 25, the shape of the blades was a circular section (is shown in figure 3.3), and the outer diameter of the runner was $D = 160mm$. Inlet angle of the blade "β_1" ranges from 10° to 24° and the outlet angle of the blade "β_2" ranges from 80° to 100°. The width of the runner and nozzle were the same, $w = 35mm$, thinner than what is usually found in other studies [5, 7, 10]. The nozzle entry arc on the prototypes is $\theta = 110°$. The inlet pipe and the nozzle are horizontally installed. A summary with the prototypes geometrical configuration is presented in table 3.1.

Runner	Inlet Angle $\beta_1[°]$	Outlet Angle $\beta_2[°]$	Runner blades
A	24	100	25
B	10	80	25
C	24	80	15
D	10	100	15

Table 3.1: Cross flow turbine prototypes tested

(a) Lateral view

(b) Front view

(c) Isometric view

(d) Section view
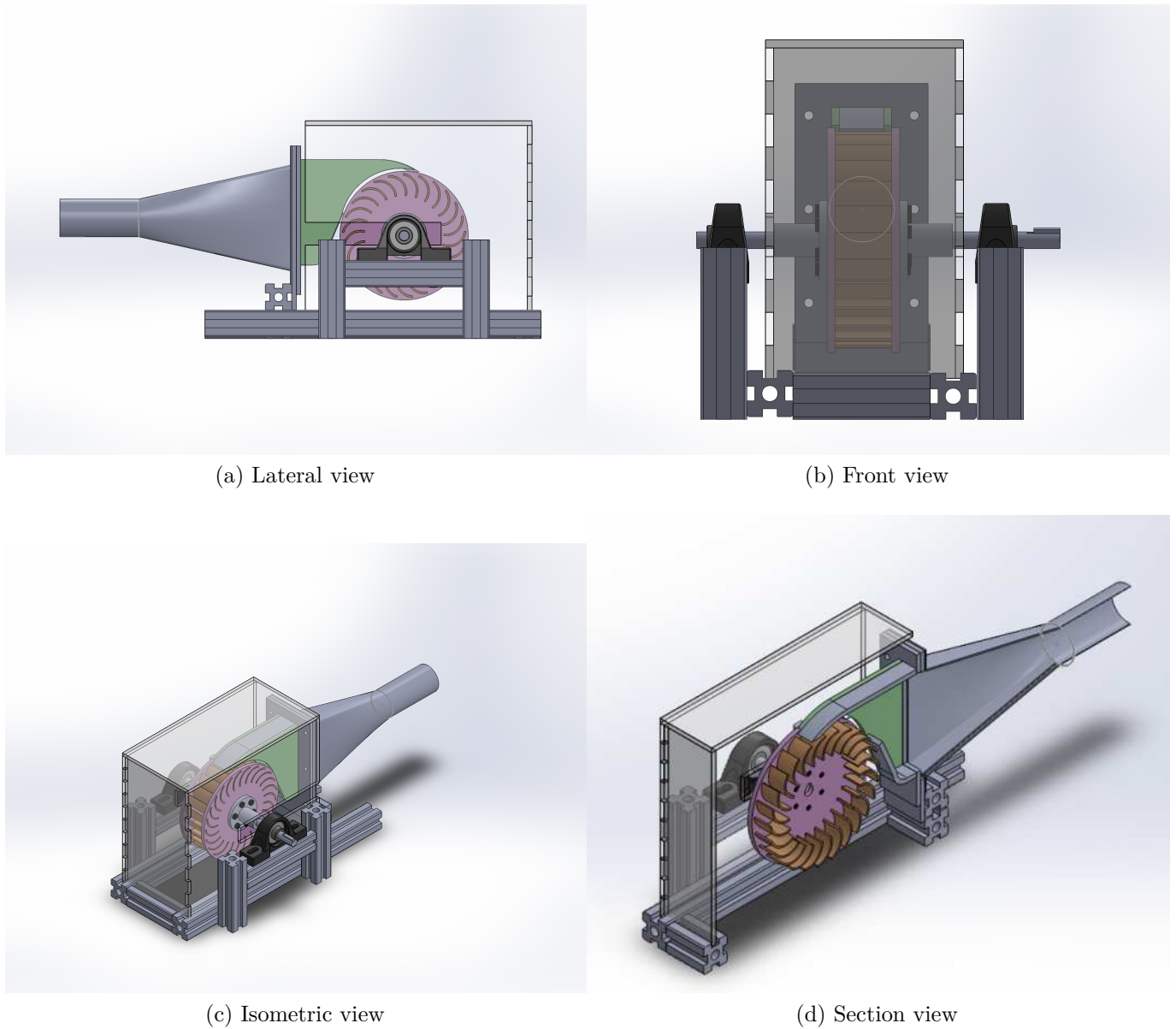
Figure 3.1: Cross flow turbine prototypes 3D Model
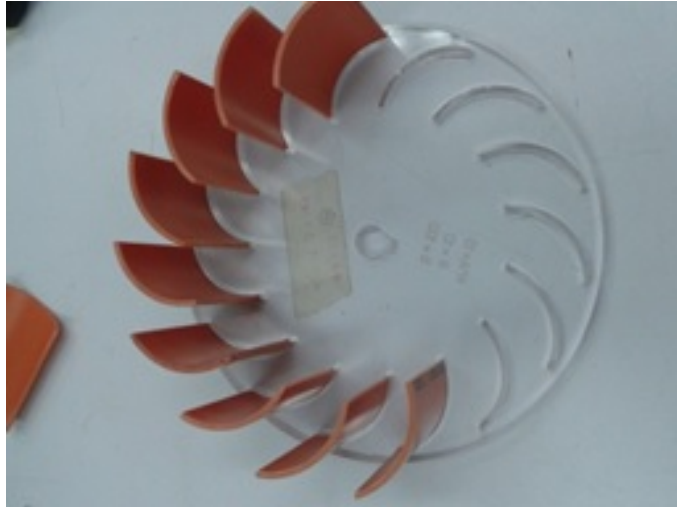
(a)
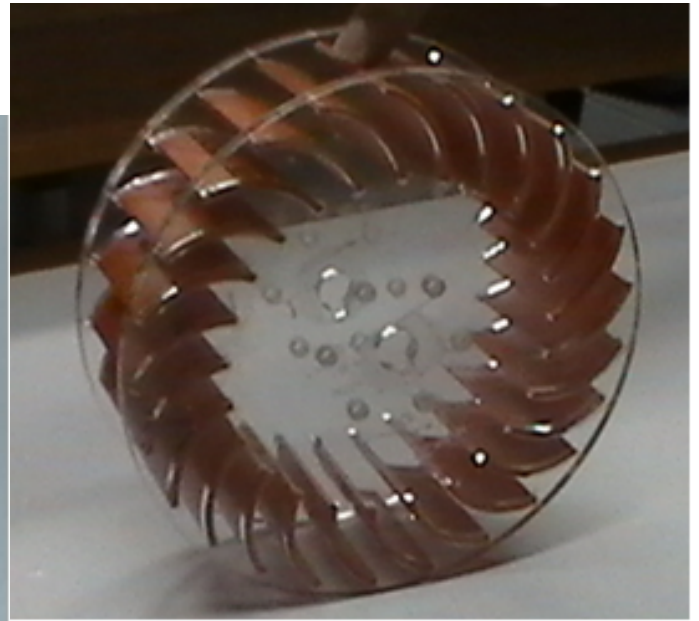
(b)
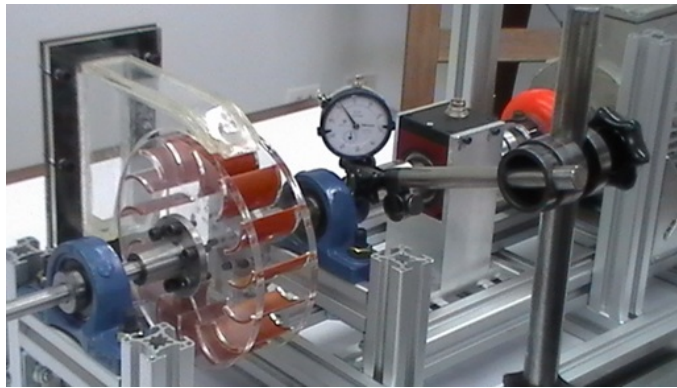
(c)
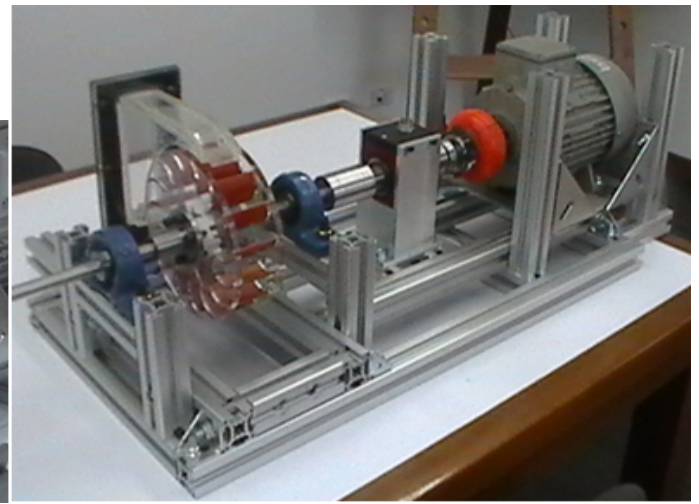
(d)

Figure 3.2: Some pictures of the constructive process

(a) Runner A

(b) Runner C

(c) Runner D

(d) Runner B
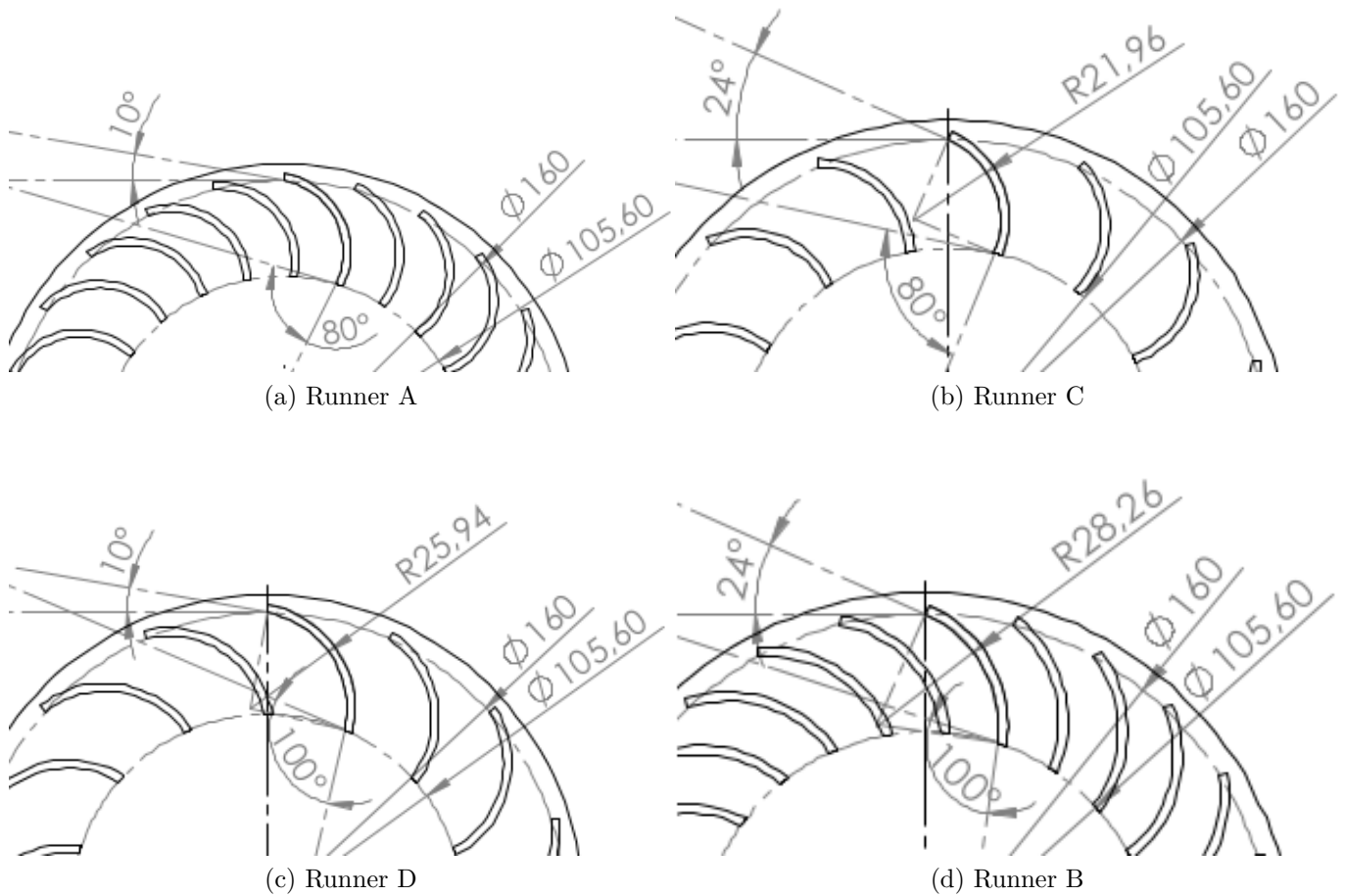
Figure 3.3: Blade geometry

3.2.   Experimental setup

The cross flow turbine prototypes were tested in the Hydraulics Laboratory at Eafit University. A pump in the basement of the building pumps water from a deposit into a hydraulic loop, to which the prototypes were connected. The outlet flow of water from the turbine went back to the deposit. The physical experimental assembly is shown in figure 3.4. The pressure was regulated by a valve located upstream the turbine and the flow rate was modified by the pump rotational speed. The testing bench built and used in the tests is shown in figure 3.5
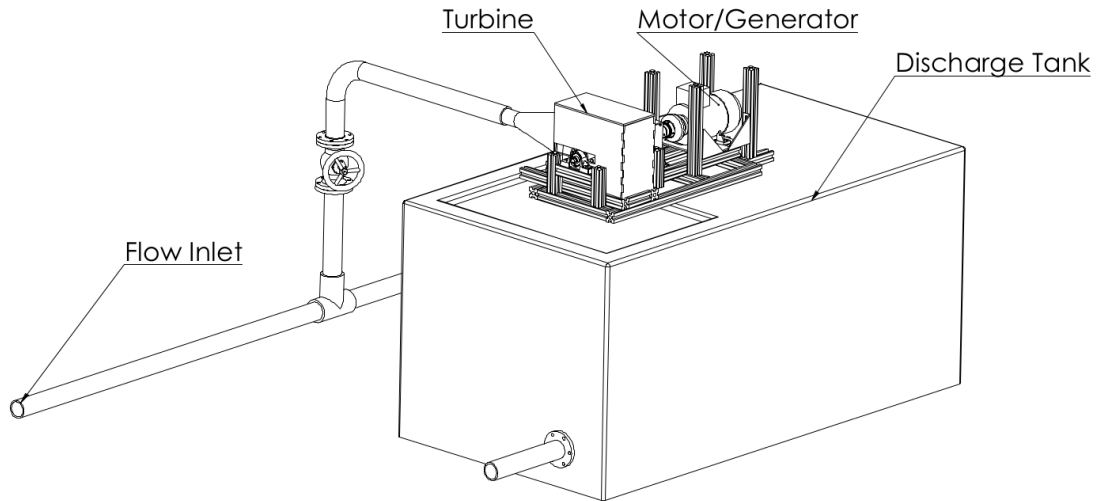
Figure 3.4: Experimental assembly

3.3.   Experimental equipment

The cross flow turbine prototypes were instrumented with a pressure transmitter, a dynamic torque sensor with a built in encoder and a flow meter in order to calculate the efficiency. A Krohne Enviromag 2100 electromagnetic flow meter was connected to the hydraulic loop that delivers the water to the turbine. A pressure transmitter WIKA $s-10$ measured the differential pressure between the atmospheric pressure and the turbine inlet. A Futek TRD605 torque sensor was used to measure the shaft torque and to count the rotational speed of the runner. The range and other parameters of the equipment are summarized in table 3.2

A National Instruments CompactRio 9075 with modules NI 9402, NI 9203, NI 9213 and NI 9215 was used to log data during the experiments. A LabView program received the signals from the modules in the CompactRio and saved the results in a text file.

Equipment	Variable measured	Range	Uncertainty
Torque sensor	Shaft torque	$\pm 250 Nm$	$\pm 0.2\%$
Flow meter	Flow rate into the prototype	$0 - 55 L/s$	$\pm 0.03\%$
Encoder	Rotational speed	$0 - 7000 rpm$	$\pm 0.2\%$
Pressure transmitter	Pressure at turbine inlet	$0 - 100 psi$	$\pm 0.25\%$

Table 3.2: Experimental Equipment Summary
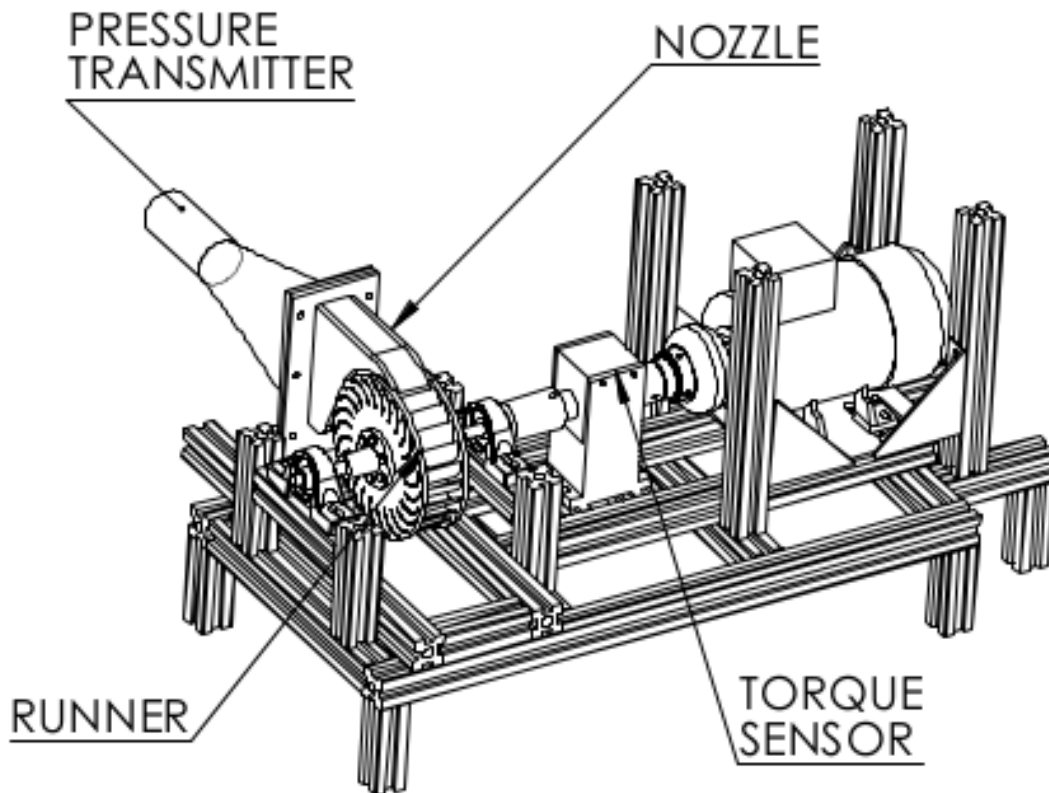
Figure 3.5: Test bench used for experiments

3.4. Test procedure

The prototypes were tested using runners A, B, C and D under different flow rates as shown in table 3.3. The desired flow rate was adjusted with the pump, which was controlled by an electronic drive. The rotational speed of the runner was recorded initially without applying any load to the turbine, then the load was applied to the turbine's shaft by means of an induction motor, whose rotational speed was controlled. The torque was recorded throughout the experiment, and the pressure was measured at the turbine inlet for every flow rate. All the variables measured were checked several times in the experiments to ensure the correct operation of the equipment, finally with the measured data the net head of the turbine was estimated as described in Hydraulic Turbines and Pump-Turbines performance test codes [33].

Runner	Flow rate [lps]	Pressure(psi)
A	14.2	3.5
A	13.2	2.0
A	11.0	2.2
A	9.5	2.0
B	18.7	1.5
B	14.4	3.6
B	11.0	3.0
C	16.0	3.3
C	14.5	3.5
C	11.0	2.6
D	14.3	2.9
D	12.8	2.9
D	11.0	3.2

Table 3.3: Test conditions

3.5.   Design of Experiments Development

The statistical design of experiments developed, consisted of two stages, in the first stage, a fractional factorial design 2^{5-2}, in which the variables that most affect the performance were identified. In the second stage, a 3^2 factorial design was performed, in which the best operation point of the turbine was found for the operation conditions and the geometrical configurations tested.

3.5.1. 2^{5-2} Fractional Factorial Design of Experiments

The first statistical design of experiments developed was a 2^{5-2} fractional factorial design. A total of 5 factors were chosen, and these were the inlet angle to the blade, the outlet angle of the blade, the number of blades, the flow rate and the rotational speed. For every factor, two levels were fixed, a minimum and a maximum. In table 3.4, it can be found a description of the selected factors and levels. The minimum and maximum value of the levels for each factor were selected based on the information available in the literature. In a 2^{5-2} fractional factorial design, a total of 8 experimental tests must be done, in which a specific combination of the levels for each factor must be established, the combinations of factors and their corresponding

levels can be found in table 3.5 [35]. In table 3.5 "−1" represents the minimum value of the level and "1" represents the maximum value of the level.

In a fractional factorial design, it is easy to express the results of the experimental tests in terms of a regression model [35]. The linear regression model is a statistical tool that allows to identify the variables that have the greatest influence on the dependent variable. Then the regression model can be used to identify the factors that most affect the response of the process, which for the present study are the performance and the output power of the turbines. It was considered that the values of the response of the process was generated by a linear combination of the values of the factors and a random term, as described in equation 5.4.

$$Y = b_0 + b_1 \cdot x_1 + b_2 \cdot x_2 + ... + b_i \cdot x_i + \epsilon \tag{3.1}$$

where Y is the response of the process, the x_i terms are the factors and the b_i are the coefficients, this coefficients are found minimizing the residual variance. Finally, after finding the factors that most affect the process response, the best operation condition can be found.

Factors	Level Min (-1)	Level Max (1)
Flow Rate (Q)	11 [lps]	14 [lps]
Rotational Speed (R)	100 [rpm]	600 [rpm]
Inlet blade angle (β_1)	10°	24°
Outlet blade angle (β_2)	80°	100°
Number of blades (N)	15	25

Table 3.4: Factors and levels description used in the 2^{5-2} Fractional Factorial Design of Experiments

	Factors				
Exp. Test	β_1	β_2	**Q**	**N**	**R**
1	-1	-1	-1	1	1
2	1	-1	-1	-1	-1
3	-1	1	-1	-1	1
4	1	1	-1	1	-1
5	-1	-1	1	1	-1
6	1	-1	1	-1	1
7	-1	1	1	-1	-1
8	1	1	1	1	1

Table 3.5: Experimental Tests setup for calculating effects in the response variable with a 2^{5-2} design

3.5.2. 3^2 Factorial Design

After finding the more influential factors in the performance and power output of the CFT prototypes, the two more representative were selected to perform a complete 3^2 factorial design, in which a third level was selected with an intermediate value between the previously defined levels. The remaining three factors were left constant for the values taken in the prototype, in which the best performance was obtained. The objective of this experiment design was to find the best operations by condition constructing a response surface with the obtained results.

The regression model that relates the response y to the factors x_1 and x_2 is described in equation 3.2. The addition of a third level for each factor allows the design factors to be modeled as quadratic.

$$y = b_0 + b_1 \cdot x_1 + b_2 \cdot x_2 + b_{12} \cdot x_1 x_2 + b_{11} \cdot x_1^2 + b_{22} \cdot x_2^2 + \epsilon \qquad (3.2)$$

In a complete 3^2 factorial design, a total of 9 experimental tests must be done. In table 3.6, the setup of the experimental tests is described, every factor can take 3 values (levels), which in the table are described by a 1 for the maximum value, a 0 for the intermediate value and a -1 for the minimum value.

Finally, the results obtained in the 3^2 factorial design, allowed to obtain a response surface in which the best operation point for the parameters selected can be determined.

	Factors	
	x_1	x_2
	-1	-1
	0	-1
	1	-1
Levels	-1	0
	0	0
	1	0
	-1	1
	0	1
	1	1

Table 3.6: 3^2 factorial design experimental setup description

4

CFD Analysis

Additional to the experimental tests, a set of CFD simulations were performed to study the behavior and performance of the CFT and the nozzle by itself. The objective of the simulations was to study flow patterns, water velocity distribution and pressure inside the turbines. Finally the numerical results were compared with the experimental results to validate the CFD model. Ansys CFX was used to perform the simulation and analysis of the turbines, this is a high level software for general purpose in CFD analysis. The simulations were configured for each of the runners tested experimentally with a flow rate of $13L/s$ and runner rotational speeds of $100rpm$, $250rpm$, $400rpm$ and $550rpm$. The main characteristics of the analysis are listed below:

- Two phase simulations

- Three dimensional domain

- Rotating and stationary domains

- Non-structured hybrid mesh

4.1. CFD simulation process

The complete process to perform one simulation is described in this section. The process is composed by the CAD modeling of the domain, meshing of the fluid domain, physical setup and post processing. The figure 4.1 shows a CFD case in ANSYS Workbench ready to run.
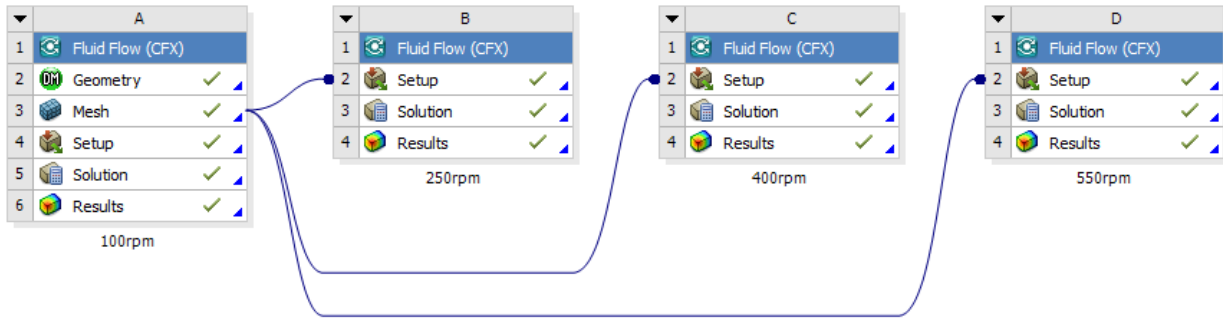
Figure 4.1: CFD case overview in Ansys Workbench

4.2.   CAD Modeling

The fluid domain was initially modeled using Solidworks and later it was imported in ANSYS own CAD modeling application, DesignModeler. Figure 4.2 shows the completed CAD model of the turbine, the rotating and stationary domains were modeled separately and assembled later. In the simulations, the nozzle and the case were a stationary domain that will be fixed in their position, while the runner was a rotating domain and rotate during the simulation.

4.3.   Meshing

The mesh of the fluid domain consists mostly of hexahedral elements with some wedges elements, it was generated using ANSYS own mesh generator application, "Meshing". The nozzle and the runner had a more refined mesh as shown in figure 4.3 aiming for a high quality results in these components. Additional mesh information is described in table 4.1

Number of Elements	Number of Nodes	Hexahedra	Wedges
146307	169098	144785	1522

Table 4.1: Mesh information
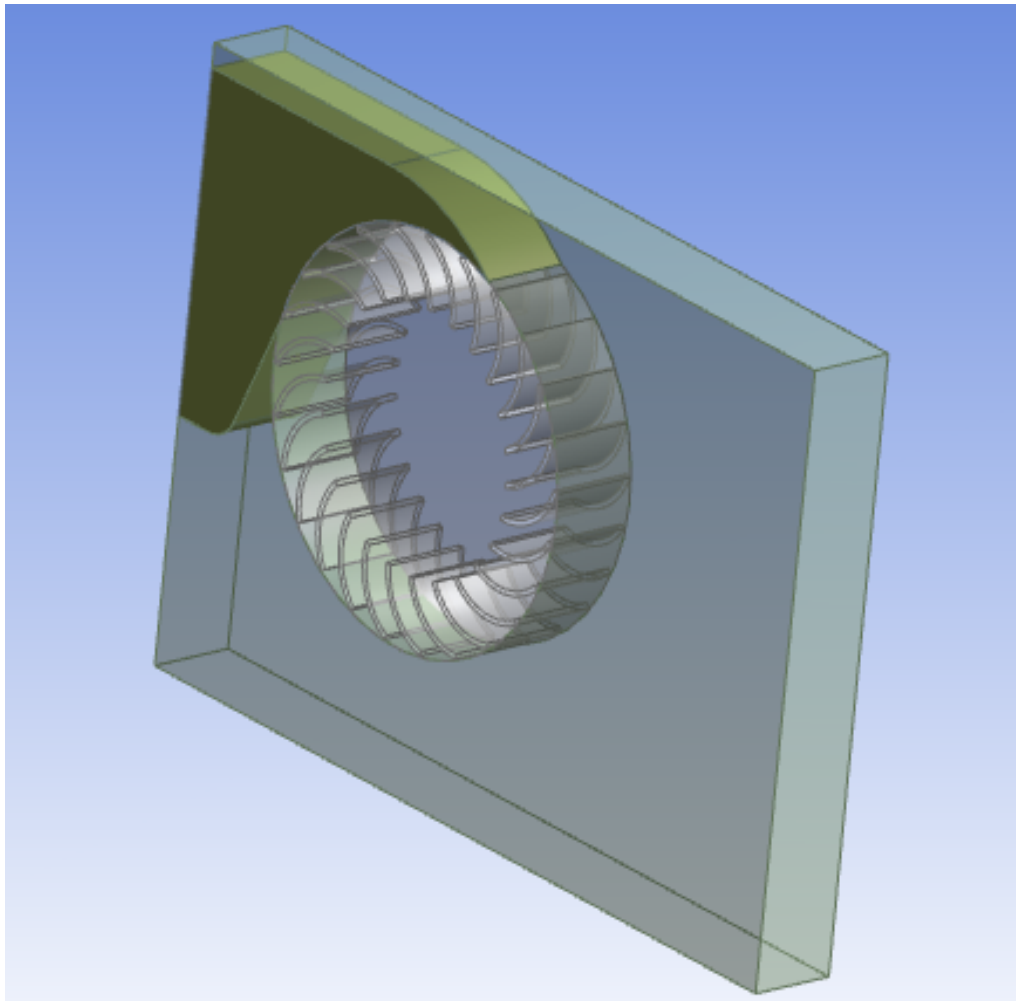
Figure 4.2: Assembly of the turbine CAD model in DesignModeler

4.4.   Physical setup

In this section, a basic configuration of the "ANSYS Pre" is presented. The essential physical setup of the problem is defined in this application, as analysis type, domains and boundary conditions.

4.4.1.   Analysis type

In "ANSYS Pre" there is a tab called "Analysis Type" that can be found editing "Flow Analysis". There can be defined whether the simulation is transient or steady state, time and control simulation. In this case the steady state option was selected.
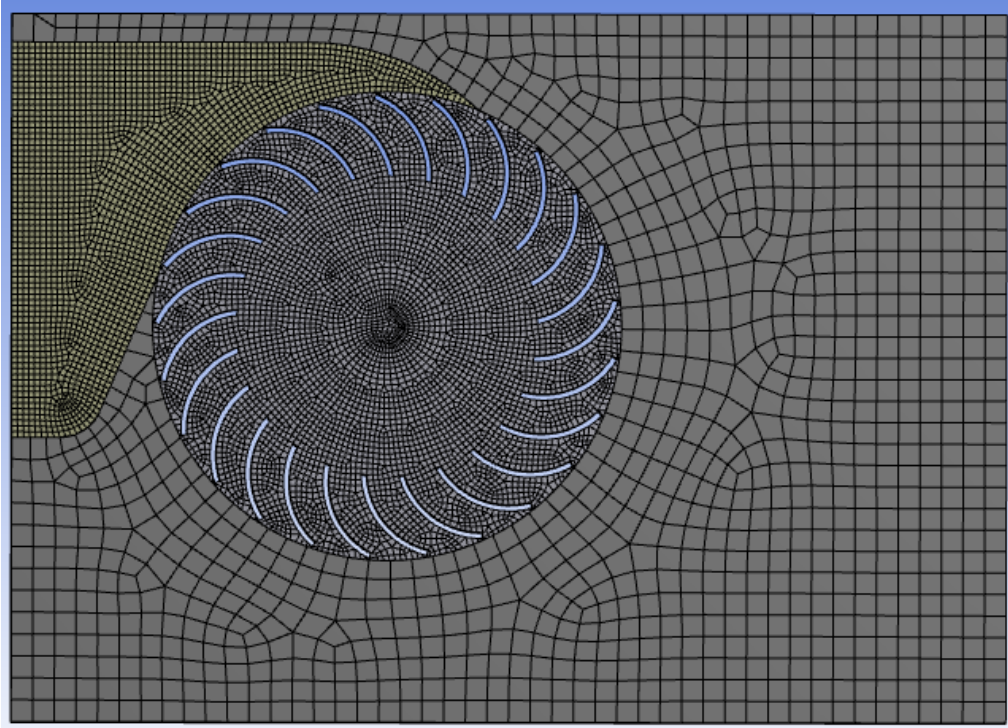
Figure 4.3: Turbine mesh

4.4.2. Domains

A stationary and a rotating domain were created, in both cases the free surface was considered using the homogeneous multiphase model, cross flow turbine accomplish well the requirements of this model, based on the air velocity inside the turbine is relatively low to the water jet, although this model does not apply to droplets under gravity in a gas, the flow of interest is not affected by the water droplets present in a real CFT. The standard free surface model and the $\kappa - \varepsilon$ turbulence model were chosen and the heat transfer was neglected. The cartesian velocity components were set equal to zero, a water volume fraction equal to zero and an air volume fraction equal to 1 were set for initial conditions.

4.5. Post processing

The results post processing were performed in the ANSYS Post application, the variables analyzed were pressure distribution, flow patterns inside the nozzle and the runner, water-air behavior inside the turbine and water velocity.

All the simulation parameters described above were selected to perform the simulations taking into consideration the works performed by some other authors as [15], [19], [18], [23], [24], [38]

Chapter 5

Results and Discussion

5.1. Experimental tests results

The results of the performance experiments for the cross flow turbine prototypes under tested conditions are presented for runners A, B, C and D, and are summarized in table 5.1. Figures 5.1 through 5.4 show the characteristic curves for the cross flow turbine prototypes under different flow rates. Each figure is composed by two different diagrams denoted by a and b. For example, diagram "a" show the variation of the turbine efficiency with rotational speed, and diagram "b" show the variation of power with rotational speed. These figures show that the rotational speed at maximum efficiency increases with increasing the flow rate, according to what was published by Olgun [11], who also explained how important are these operating conditions for the electric generator.

Prototype	Head at best Eff.[m]	Power Out. Max.[W]	Efficiency Max. [%]	Rot. Speed at best Efficiency [Rpm]
A	4.0	213.98	53.05	390.70
B	4.0	226.44	41.01	318.73
C	6.0	297.40	40.06	395.63
D	6.0	295.55	37.80	317.96

Table 5.1: Tests experimental results summary

A maximum output power of $297W$ was achieved in the prototype C with an efficiency of 36.9%, while the maximum efficiency obtained was of 53.05% in the prototype A, and its output power was $213.98W$. It can be seen that in the operation of the turbines under different head conditions, the efficiency variation was small, the maximum efficiency ranged from 37.80% to 53.05%. The best efficiencies were achieved between $300rpm$ and $400rpm$.

5.1.1.   Prototype A ($\beta_1 = 24°$, $\beta_2 = 100°$, number of blades $= 25$)

In figure 5.1, the characteristic curves obtained for prototype A are presented. It can be found that this prototype had the best performance of the prototypes tested, it obtained a maximum efficiency of 53.05% and had a maximum output power of 213.98W. This prototype had 25 blades, an inlet angle of the blade $\beta_1 = 24°$, and an outlet angle of the blade $\beta_2 = 100°$. These results show a different behavior when compared with Khosrowpanah [7] who found that the highest efficiency occured at about 15 or 16 blades. Nevertheless, the results obtained agree with the conclusions published by Joshi, Seshadri and Singh [9], Venkappayya and Nadim [10], whose works showed that the efficiency increased with increasing the number of blades, and that the optimum number of blades was 20 approximately.

5.1.2.   Prototype B ($\beta_1 = 10°$, $\beta_2 = 80°$, number of blades $= 25$)

The characteristic curves obtained for prototype B in the experimental tests are shown in figure 5.2. The maximum efficiency reached by this prototype was 41.01%, and it produced a maximum output power of 226.44W. This prototype had 25 blades, an inlet angle of the blade $\beta_1 = 10°$ and an outlet angle of the blade $\beta_2 = 80°$. If we consider the results obtained by Choi, Lim, Kim and Lee [18], the decrease in the performance of this prototype can be caused by the variation of the inlet and outlet angles of the blade, which are 14° and 20° lesser than in prototype A.

5.1.3.   Prototype C ($\beta_1 = 24°$, $\beta_2 = 80°$, number of blades $= 15$)

Figure 5.3 shows the characteristic curves obtained for prototype C during the experimental tests, it was found that the maximum output power was 297.40W with a maximum efficiency of 40.06%. This prototype had 15 blades, an inlet angle of the blade $\beta_1 = 10°$ and an outlet angle of the blade $\beta_2 = 80°$. These results show a lower performance compared with prototype A. The results confirm the observation made by Choi et al [15], who found that the inlet and outlet angles of the runner blades considerably affected the performance of the turbine. Again the decrease in the performance can also be caused by the input and output angles of the blade, which are 14° and 20° lesser than in prototype A. Moreover, a more drastic efficiency decrease was expected, due to the reduction of blades in the runner; a reduction in this parameter has been highlighted in many studies as one of the most important effects in the turbine performance.

5.1.4. Prototype D $(\beta_1 = 10°, \ \beta_2 = 100°,$ **number of blades** $= 15)$

Figure 5.4 shows the characteristic curves for prototype D built with the experimental data obtained in the tests, it can be found that the maximum efficiency obtained with this prototype was 37.80% which was the least efficient of the tested prototypes and its maximum output power was 295.55W. This prototype had 15 blades, an inlet angle of the blade of $\beta_1 = 10°$ and an outlet angle of the blade $\beta_2 = 100°$. The causes of the decrease in the performance of this turbine can not be determined so easily, by comparing the results obtained with the remaining prototypes. In this prototype, the few amount of runner blades may have caused an inefficient operation, but it can be seen that the other parameters also have an effect in the turbine efficiency.
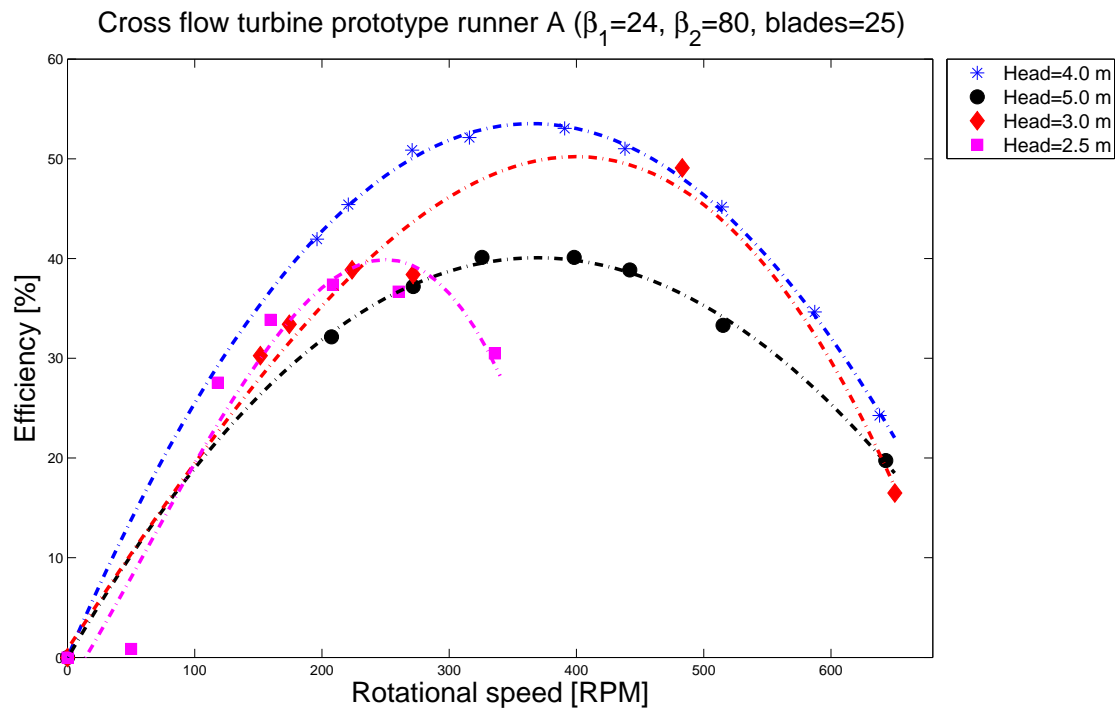
(a)
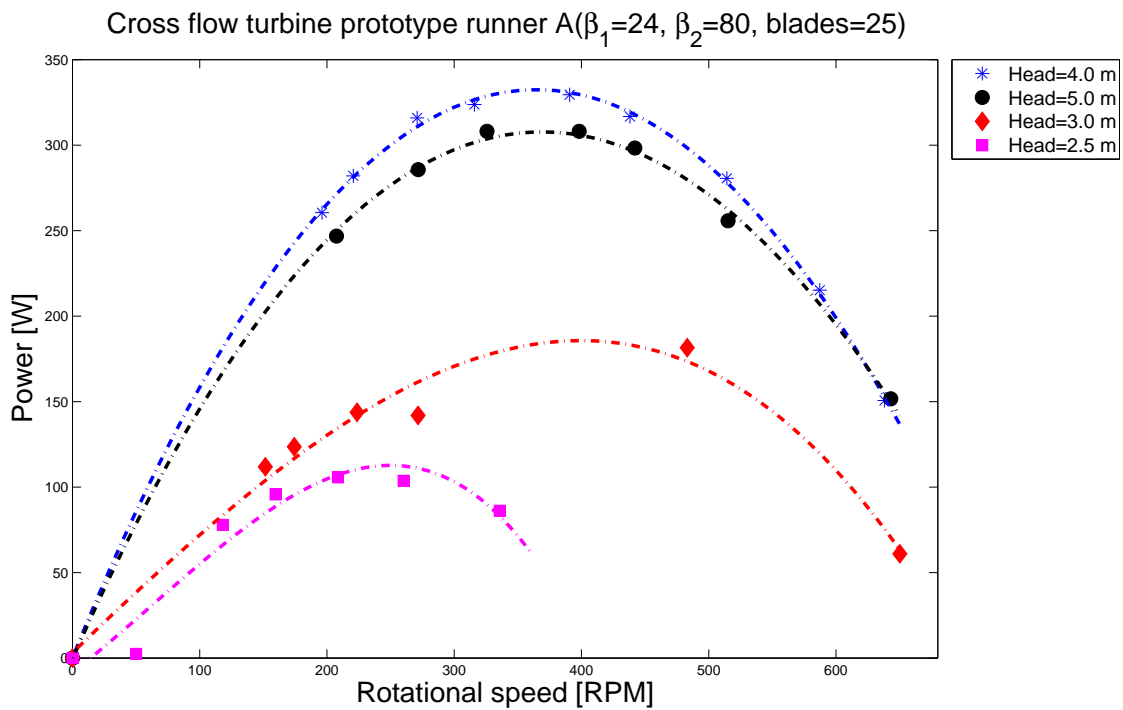
(b)

Figure 5.1: Characteristic curves of A
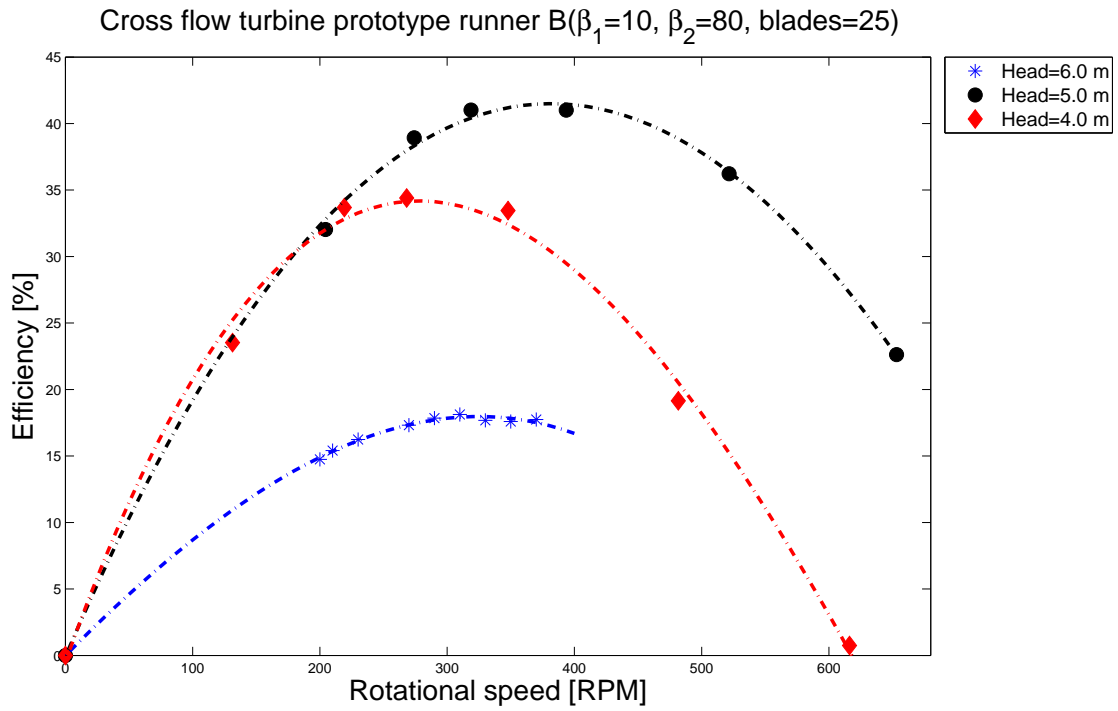
(a)
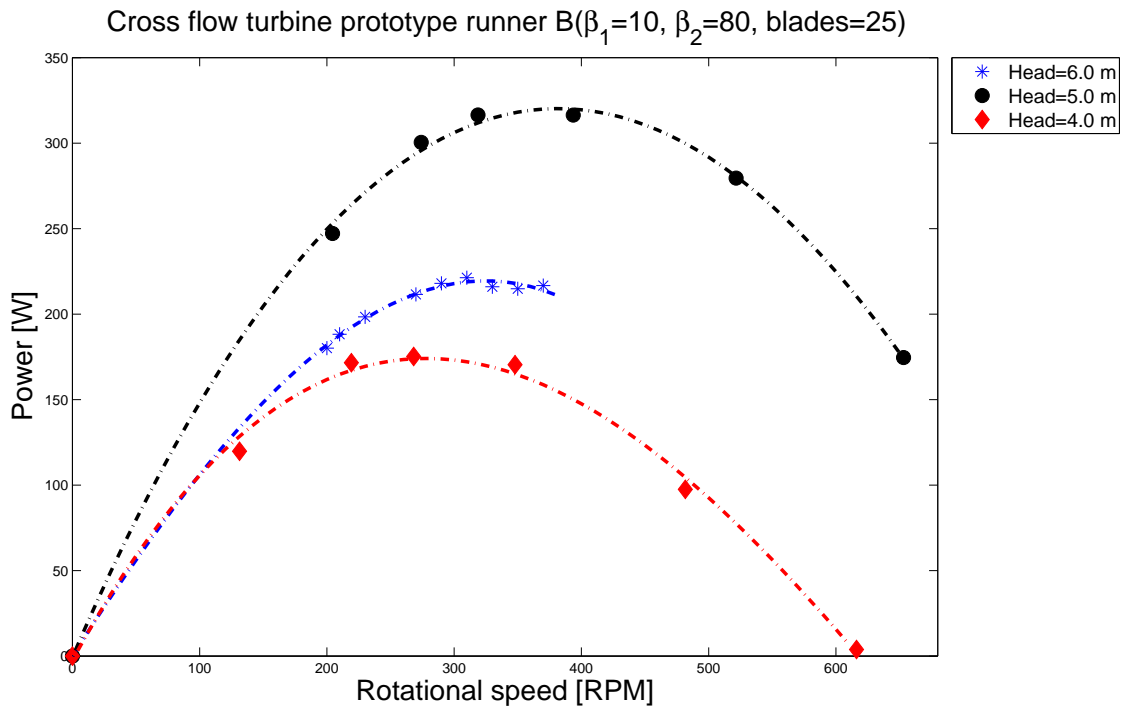
(b)

Figure 5.2: Characteristic curves of B

Cross flow turbine prototype runner C(β_1=24, β_2=80, blades=15)

(a)

Cross flow turbine prototype runner C(β_1=24, β_2=80, blades=15)
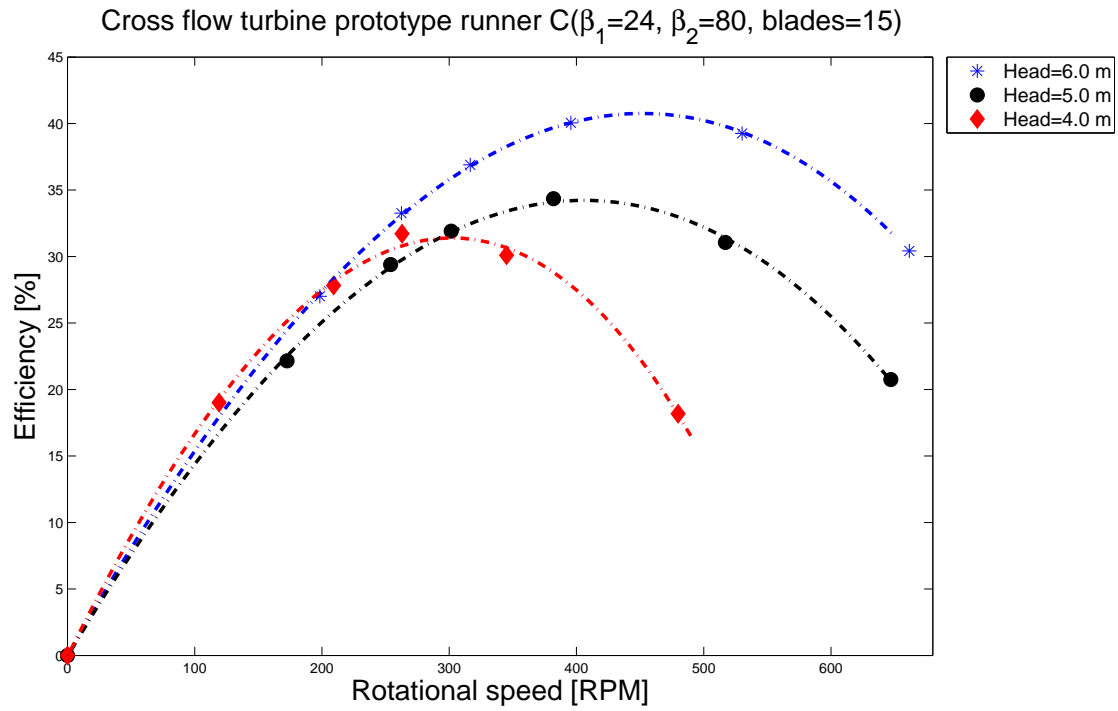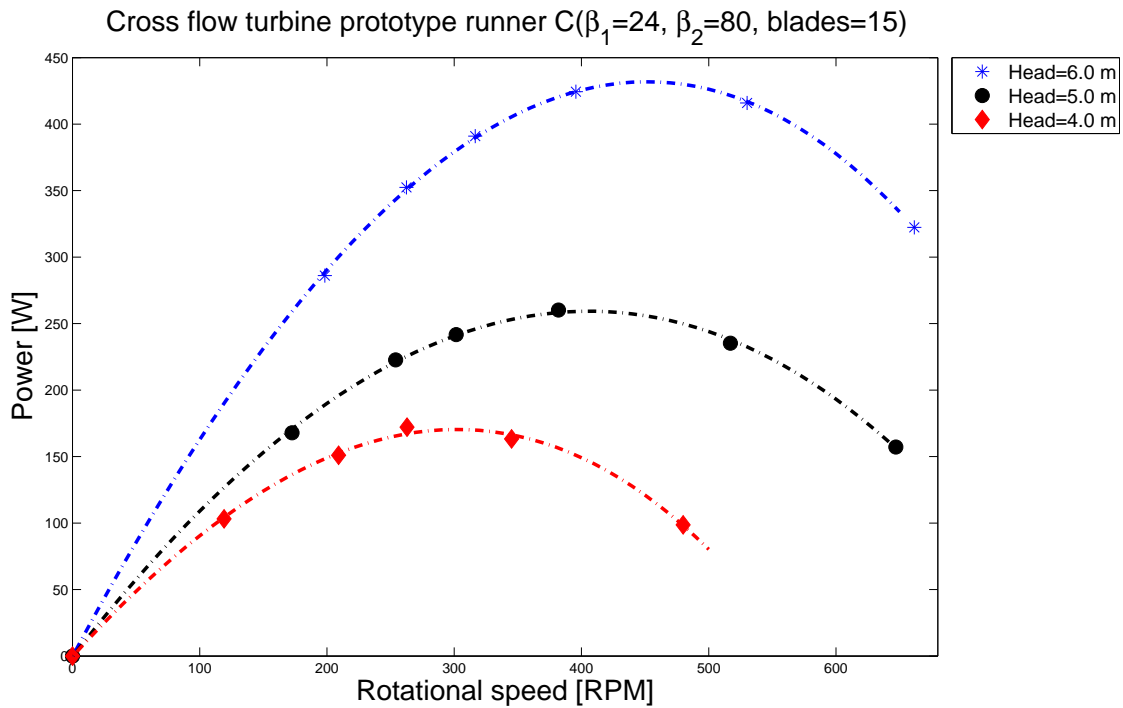
(b)

Figure 5.3: Characteristic curves of C
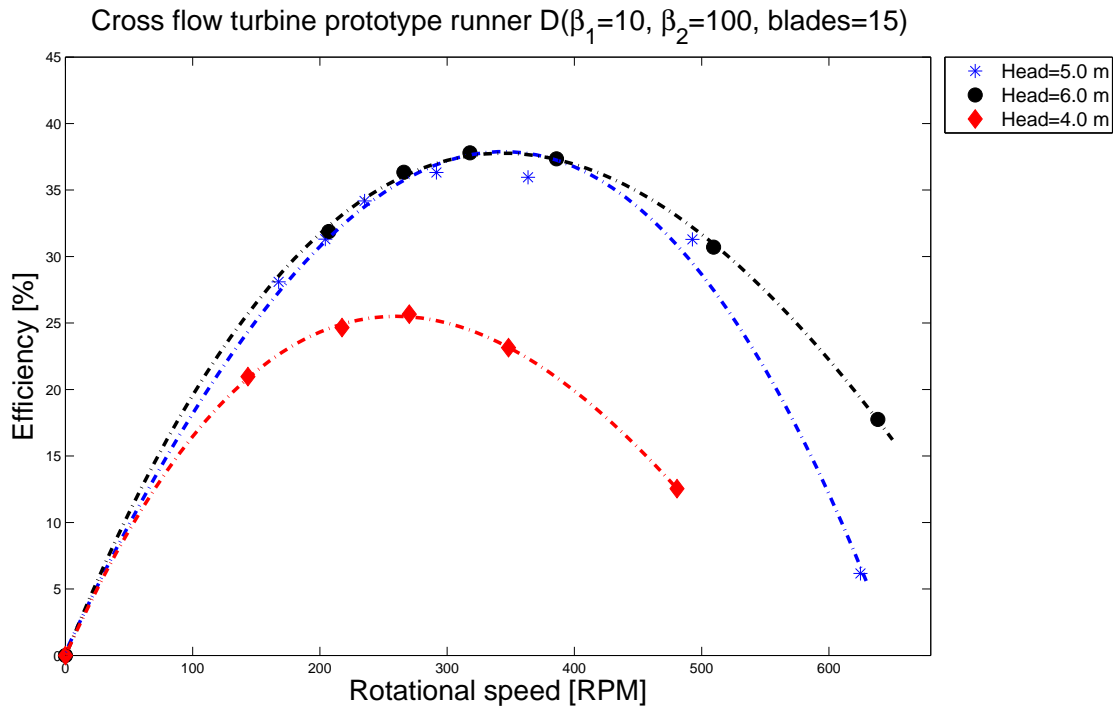
(a)
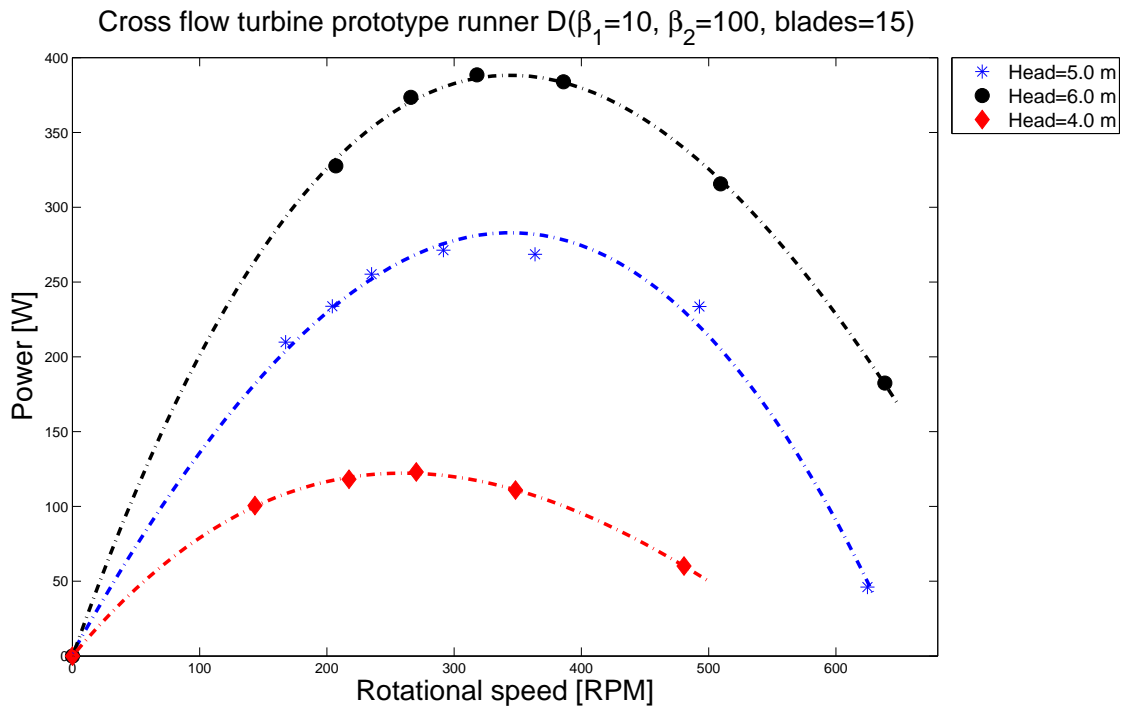
(b)

Figure 5.4: Characteristic curves of D

5.1.5.   Error analysis

Due to the fact that every physical quantity measured in experiments is subject to error there is an uncertainty in the obtained results. In this section are presented some elementary aspects of error analysis for the performed experiments. This analysis is mainly composed of the calculation of propagation of precision uncertainties.

Propagation of precision uncertainties

The propagation of precision uncertainties in measurements is governed by statistics, in this case it can be done as described in Mills and Chang article [39], where the uncertainty of a function Y of n independent measurements X_i with small uncertainties P_i can be determined as equation 5.1.

$$P_Y = [\sum_{i=1}^{n} (\frac{\partial Y}{\partial X_i} P_i)^2]^{1/2} \tag{5.1}$$

With the data collected in the experimental measurements, and the manufacturer information of the measuring equipment used, the propagation of the uncertainty for the shaft power was calculated as equation 5.2

$$P_{W_{Shaft}} = T\omega \pm [(\frac{\partial W_{Shaft}}{\partial \omega} P_\omega)^2 + (\frac{\partial W_{Shaft}}{\partial T} P_T)^2]^{1/2} \tag{5.2}$$

The hydraulic power uncertainty was calculated as equation 5.3, where P_ω and P_T are the uncertainties of the encoder and the torque sensor respectively

$$P_{W_{Hydraulic}} = HQ\gamma \pm [(\frac{\partial W_{Hydraulic}}{\partial H} P_H)^2 + (\frac{\partial W_{Hydraulic}}{\partial Q} P_Q)^2]^{1/2} \tag{5.3}$$

where P_H and P_Q are the uncertainties of the pressure transmitter and the flow rate sensor respectively. And finally the efficiency uncertainty was calculated as equation 5.4

$$P_{\eta_{Turbine}} = \frac{W_{shaft}}{W_{Hydraulic}} \pm [(\frac{\partial \eta_{Turbine}}{\partial W_{shaft}} P_{W_{shaft}})^2 + (\frac{\partial \eta_{Turbine}}{\partial W_{Hydraulic}} P_{W_{Hydraulic}})^2]^{1/2} \tag{5.4}$$

where $P_{W_{Shaft}}$ and $P_{W_{Hydraulic}}$, are the uncertainties of the shaft power and the hydraulic power previously calculated. In table 5.2 the results of the uncertainties mentioned above

for the prototypes tested are shown, this uncertainties were calculated in the best efficiency operation point obtained.

Prototype	Shaft Power Uncertainty$[W]$	Hydraulic Power Uncertainty$[W]$	Efficiency Uncertainty$[\%]$	Max. Efficiency $[\%]$
A	±2.168	±2.268	±1.098	53.05
B	±1.980	±2.438	±0.823	41.01
C	±2.324	±2.709	±0.786	40.06
D	±1.911	±2.421	±0.902	37.80

Table 5.2: Precision uncertainties propagation results

5.2.   Design of experiments results

In this section the results of the performed design of experiments are presented. A fractional factorial design 2^{5-2} was implemented in which the variables that most affect the response of the process were found. The variables studied were operational conditions as the flow rate and the runner rotational speed. Geometrical parameters of the turbine, as the inlet angle to the blade, outlet angle of the blade and the number of blades, were also considered as variables of study in this statistical design of experiments. The response of the process studied were the performance and the power output of the turbines.

The results of the fractional factorial design 2^{5-2} showed that the variables that most affected the performance and the power output of the turbine prototypes were the flow rate and the runner rotational speed. With these results, a complete 3^2 factorial design was performed. In this case, just the prototype with the maximum performance obtained was studied. The variables analyzed were again the flow rate and the runner rotational speed, but in this case three levels were selected. For this configuration a total of 9 experimental tests were performed. With the results of the 3^2 factorial design, a surface response was obtained and the best operational point of the turbine for the conditions tested was identified.

5.2.1.   Fractional factorial design 2^{5-2} results

In this experimental methodology, a total of 5 variables were selected for every prototype these variables were the flow rate, the inlet angle to the blade, the outlet angle of the blade, the runner rotational speed and the number of blades. For every variable two levels were assigned,

Exp. test	Variables					Responses	
	Angleβ_1	Angleβ_2	Flow rate[l/s]	Blades	Rot. Speed [rpm]	Power [W]	Eff.
1	10	80	11	25	600	2.30	0.74
2	24	80	11	15	100	19.02	19.02
3	10	100	11	15	600	0.00	0.00
4	24	100	11	25	100	75.08	30.26
5	10	80	14	25	100	189.56	32.03
6	24	80	14	15	600	130.07	20.75
7	10	100	14	15	100	179.94	31.88
8	24	100	14	25	600	113.13	19.74

Table 5.3: 2^{5-2} fractional factorial design experimental setup

a minimum and a maximum. With the setup previously described a total of 8 experimental tests were performed, the setup of each experimental test can be found in table 5.3. for every test the efficiency and the power output of the CFT prototypes were registered.

In this study, the highest performance and the highest power output were obtained with the turbine with an inlet angle to the blade of 10°, an outlet angle of the blade of 80°, and 25 blades. This output power and efficiency were obtained by this turbine operating at $100rpm$ and a flow rate of $14l/s$.

From the results obtained, a multiple linear regression was developed, with the objective to determine the effect of the variables studied in the efficiency and the power output of the turbine. In tables 5.4 and 5.5, the results of the linear regression can be found. Based on the "p-value", the variables that most affect the performance of the turbine can be determined by identifying the factors with a "p-value" less than 0.05. In this case, the flow rate and the runner rotational speed were the factors with the higher impact in the efficiency and power output of the CFT prototypes.

This study was developed with the statistical software R version 3.02. With these results it was decided to perform a complete factorial design for the turbine in which the best performance was obtained. In this second design of experiments, the geometrical parameters of the prototype remained constant, and for the flow rate and runner rotational speed which were the variables that most affected the efficiency and the power output of the prototype, three levels were selected. Considering this, a 3^2 factorial design was developed for this case.

Multiple linear regression for the Efficiency			
Intercept	Estimate	t value	p value
	19.302	12.591	0.00625
Angle β_1	3.140	2.048	0.17709
Angle β_2	1.168	0.762	0.52587
Flow rate	6.797	4.434	0.04728
Blades	1.390	0.907	0.46027
Rot. Speed	-8.995	-5.867	0.02784

Table 5.4: Multiple linear regression results for the turbine output efficiency

Multiple linear regression for the Output Power			
Intercept	Estimate	t value	p value
	88.637	9.665	0.0105
Angle β_1	-4.312	-0.470	0.6845
Angle β_2	3.400	0.371	0.7464
Flow rate	64.537	7.037	0.0196
Blades	6.380	0.696	0.5586
Rot. Speed	-27.263	-2.973	0.0970

Table 5.5: Multiple linear regression results for the turbine output power

5.2.2. Factorial design 3^2 results

In this section, the design of experiments performed with the prototype in which the best performance was obtained, is described. The statistical design of experiments performed in this case was a complete 3^2 factorial design. For this design, the geometrical parameters of the prototype remained unchanged because, as was found previously, this variables have the least impact in the CFT prototype performance, however this observation can only be considered for the conditions established in this design of experiments. On the other hand, it was found that the flow rate and the runner rotational speed significantly affected the efficiency and the output power of the turbine. For each of this 2 variables, 3 levels were selected, 2 of the levels were the same that were used in the 2^{5-2} fractional factorial design, those levels were $11L/s$ and $14L/s$ for the flow rate, and, for the runner rotational speed, the levels were $100rpm$ and $600rpm$. Additionally a third level was selected, this level took an intermediate value of $13L/s$ for the flow rate, and a value of $400rpm$ were selected for the runner rotational speed.

Exp. Test	Variables		Responses	
	Rot. Speed [rpm]	Flow rate [L/s]	Efficiency [%]	Power [W]
1	100	11	30.26	75.08
2	400	11	49.09	121.82
3	600	11	16.49	40.91
4	100	13	41.94	158.10
5	400	13	53.05	199.97
6	600	13	24.26	91.46
7	100	14	32.14	184.17
8	400	14	40.12	229.90
9	600	14	19.74	113.13

Table 5.6: 3^2 fractional factorial design experimental setup

A total of 9 experimental tests were performed with this methodology, the characteristics of the tests can be found in the table 5.6. The results obtained in each experimental test for the efficiency and the output power of the prototype, can also be found in the table 5.6. The maximum efficiency value obtained was 53%, the flow rate at this point was $13L/s$, the runner rotational speed was $400rpm$, and the output power was $200W$. On the other hand, when the turbine operated at rotational speed of $400rpm$, and flow rate of $14L/s$, a maximum power output of $230W$ was obtained, and the efficiency in this operation point was of 40.12%

5.2.3.   Efficiency and Power response surface

From the results obtained in the 3^2 fractional factorial experiment design, a combination of the rotational speed and flow rate were found to obtain both, the maximum efficiency and the maximum power output in the prototype tested. However, this combination of the variables do not necessarily correspond to the best operating point of the turbine. The best operating point is bounded by the set of conditions where this equipment can be operated [34].

With the results of the experimental procedure described above, a response surface for the efficiency and the power output were determined, this was performed using the statistical package "R". The response surfaces obtained can be found in figures 5.5, and 5.6. Both figures are composed of two images, the image (a) shows the 3D response surface, and the image (b) shows a contour of the response surface.

According to the results obtained in the experimental tests, and based on the efficiency response surface (fig 5.5), the best efficiency can be obtained operating the turbine in a range

Response Surface Flow Rate [Lps] vs Rotational Speed [RPM]
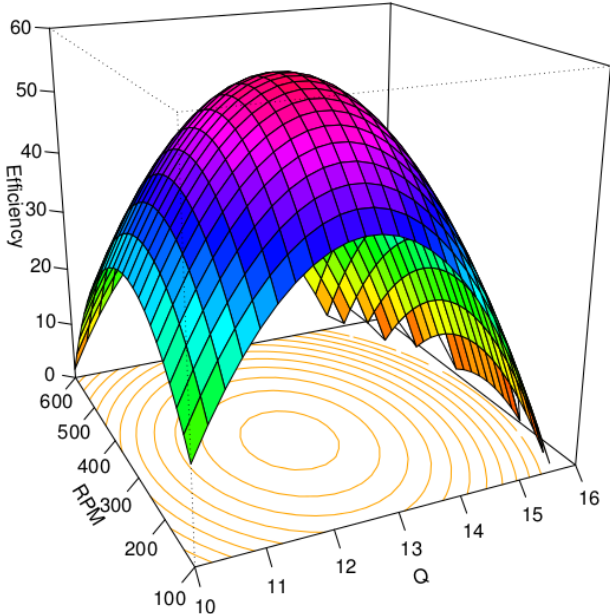
(a)

Contour Diagram Rotational Speed [RPM] vs Flow Rate [L/s]
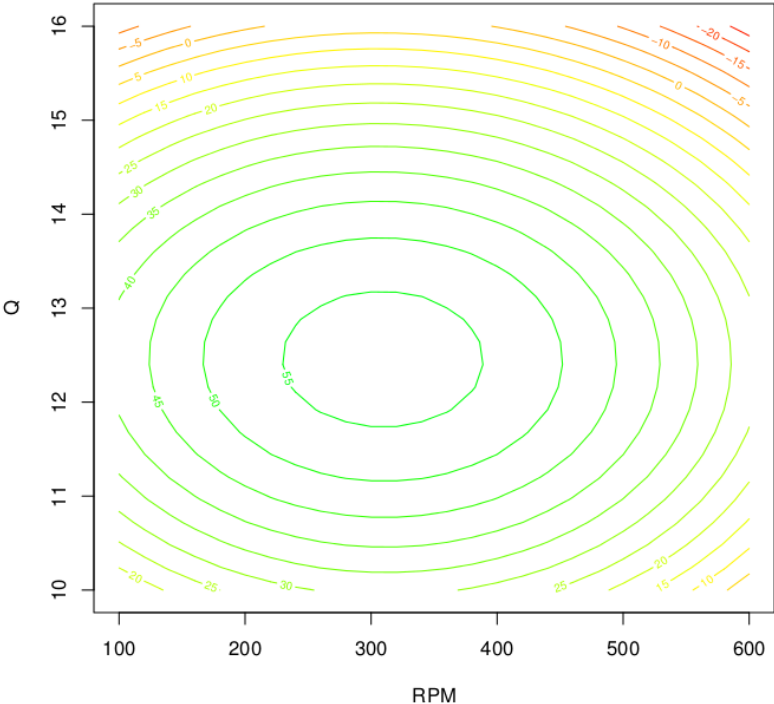
(b)

Figure 5.5: Efficiency response surface

Power Response Surface Flow Rate [Lps] vs Rotational Speed [RPM]

(a)

Power Contour Diagram Rotational Speed [RPM] vs Flow Rate [L/s]

(b)

Figure 5.6: Output power response surface

of flow rate between $12L/s$ and $13L/s$, and the runner rotational speed range between $250rpm$ and $400rpm$. Finally a maximum efficiency of 55% could be reached with this operating conditions.

In the power surface response (fig 5.6), it can be found that the maximum output power could be obtained when the turbine is operated in a flow rate range between $16L/s$ and $20L/s$, and the runner rotational speed range between $200rpm$ and $350rpm$. The estimated power under this operating conditions is $280W$.

5.3.   CFD analysis results

Fluid dynamic simulations were performed for every prototype model to show the flow characteristics inside the cross-flow turbine. The water flow rate defined for every model was $Q = 13L/s$, every wall in the model such as the case, runner blades, runner side disks and nozzle walls were set as walls with no slip condition. The free surface homogeneous model was selected to model water and air phases and a $k - \varepsilon$ turbulence model was applied. The computational domain was divided in two sub-domains: the runner as a rotating domain and the nozzle and case as a static domain, with a general connection condition as interface model between both sud-domains. At the nozzle inlet a water volume fraction of 1 was set, while in the base of the casing opening condition was imposed with a pressure of $1atm$ [40] .

5.3.1.   Turbine qualitative flow field analysis

Figures 5.8 through 5.11 show velocity vectors of the flow field inside the turbine model operating at different rotational speed. The velocity vectors are shown using absolute velocity variable in the fluid domain of turbine model. It can be seen that the flow pattern in the internal area of the runner is dominated by the runner rotational speed and the runner geometrical configuration. It can also be found that the water velocity becomes accelerated while passing along the nozzle. After its pass through the runner first stage, the flow is accelerated again and then the water enters into the runner second stage, and finally leaves the turbine. It can also be seen that the velocity vector angle at the outlet of the first stage blades is different from the velocity vector angle at the inlet of the second stage blades.

These parameters are considered to have the same value during the hydraulic design in the turbine velocity diagrams, assuming an ideal turbine operation, looking for the grater hydraulic energy conversion [5]. This makes that the knowledge of the real velocity triangles for each stage of the turbine becomes of great importance. It is also important to note that the

absolute water velocity angle (α), which is also assumed constant in the runner first stage inlet, varies along the nozzle outlet, as shown in detail in figure 5.7, this makes that the velocity triangles are also different in several sections of the runner.This characteristic is very difficult to determine experimentally and CFD analysis becomes advantageous in this case.

Velocity vectors, velocity and pressure distributions

Figures 5.12 through 5.15 shows the contours of water velocity and water volume fraction of the turbine prototypes for different runner rotational speeds ($100rpm$, $250rpm$, $400rpm$ and $500rpm$). In the water volume fraction images, can be seen a very well defined free surface interface between the water flow and the air in the lower part of the turbine. However, these figures shows that water starts to flow over the casing walls for every rotational speed operation condition, this behavior is attributed by other authors to the recirculating flow in the second stage [23]. From $100rpm$ to $550rpm$ differences in the zones occupied by the water within the runner and the case can be observed. When the runner rotational speed increases the sector occupied by the water flow in the runner and in the case decreases.

In the same figures, it can also be seen that the flow is accelerated in the nozzle outlet, and the same behavior is found in all the small areas where the water flows, in this zones the water velocity increases in order to conserve the flow rate through the turbine. At low runner rotational speeds, a well defined first and second stage can be seen.
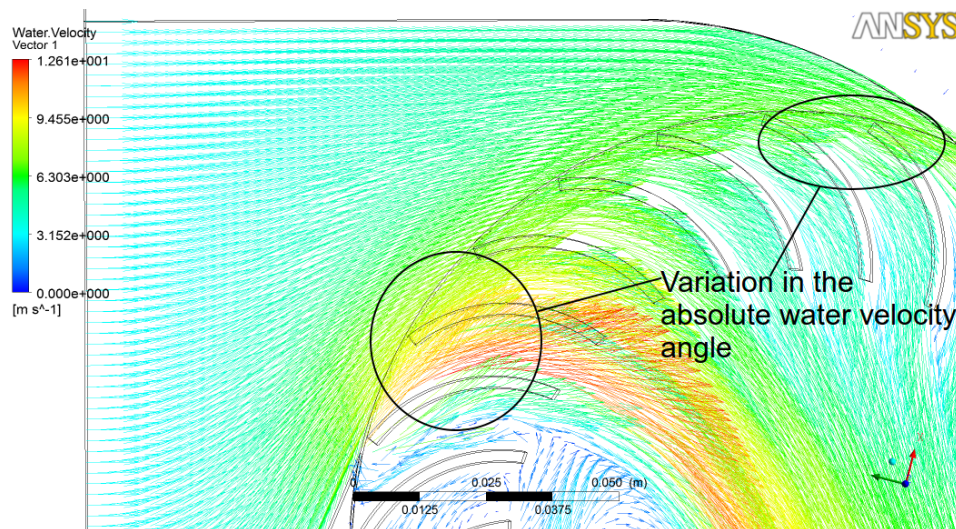
Figure 5.7: Water absolute velocity vector in the nozzle outlet
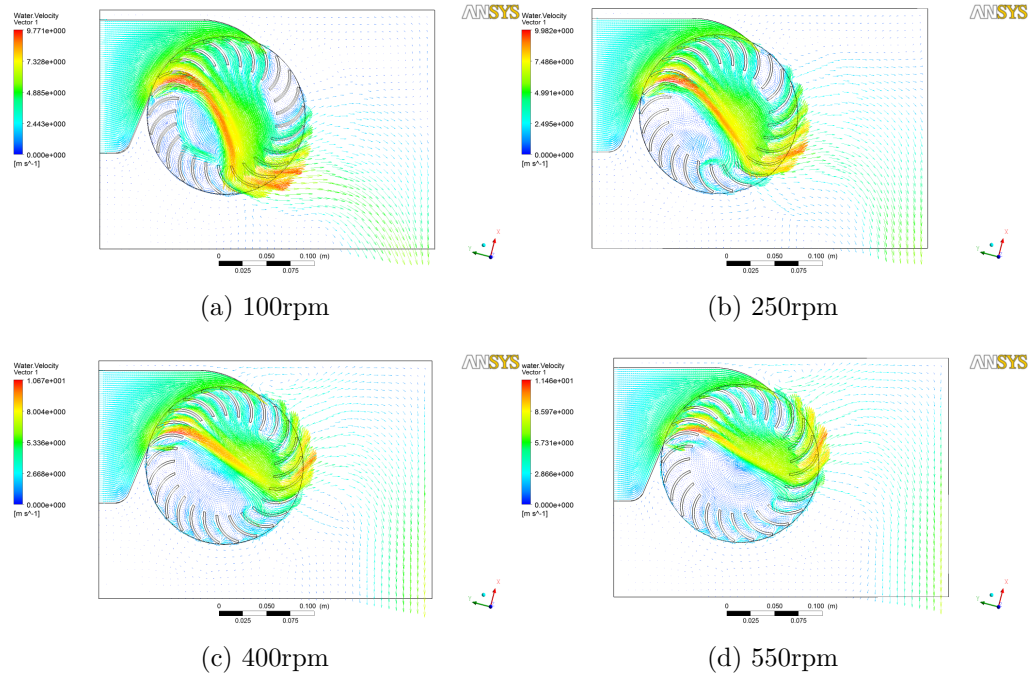
Figure 5.8: Prototype A velocity vectors variation with rotational speed
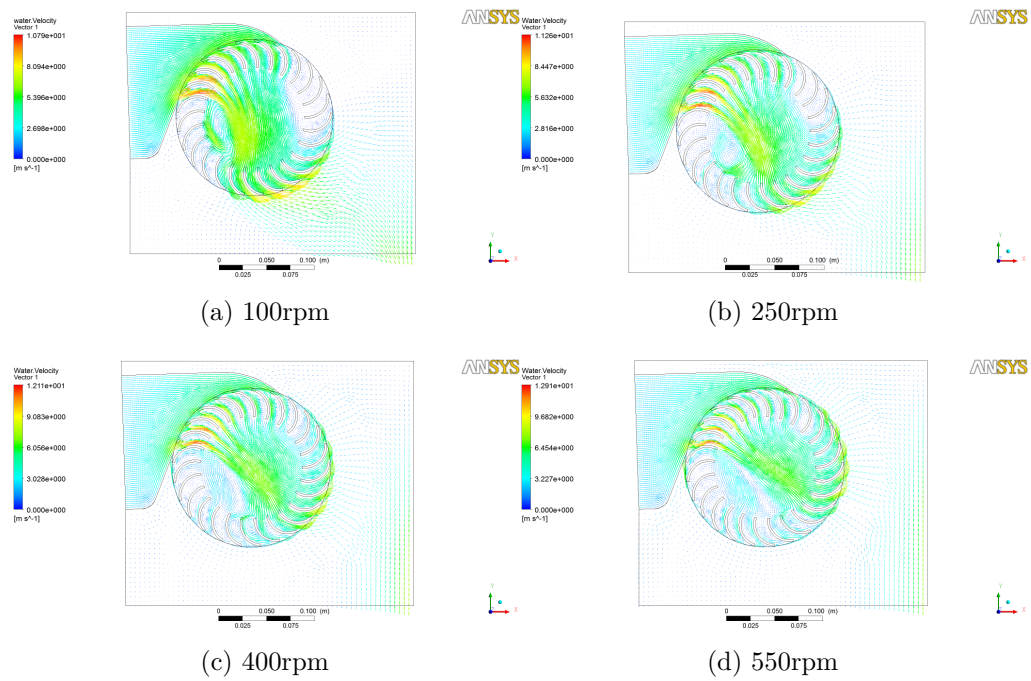
Figure 5.9: Prototype B velocity vectors variation with rotational speed

(a) 100rpm

(b) 250rpm

(c) 400rpm

(d) 550rpm
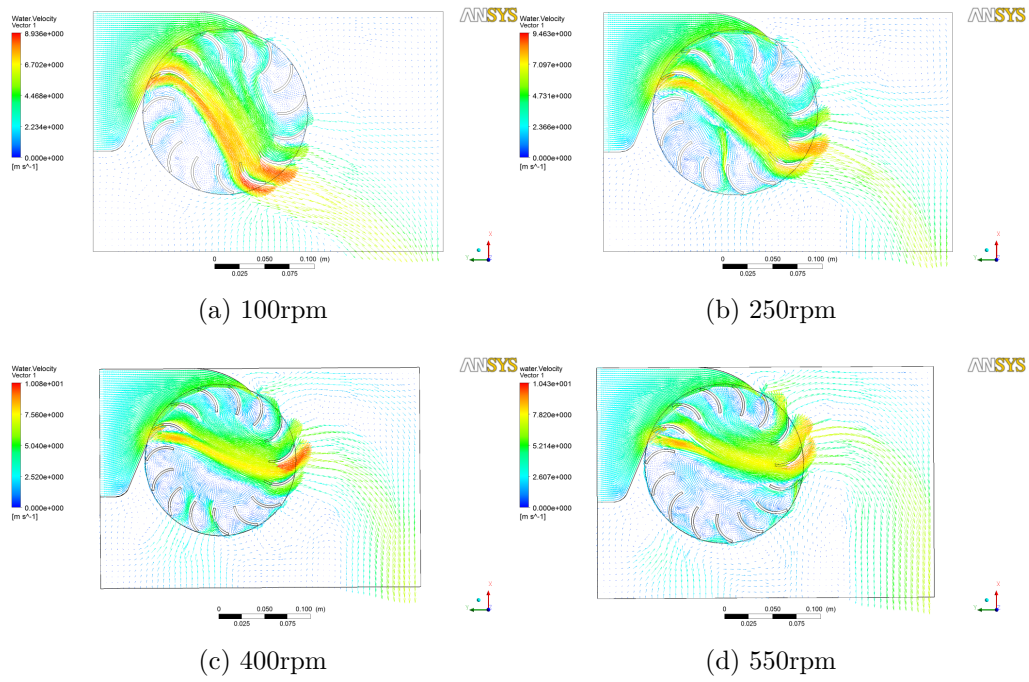
Figure 5.10: Prototype C velocity vectors variation with rotational speed

(a) 100rpm

(b) 250rpm

(c) 400rpm

(d) 550rpm
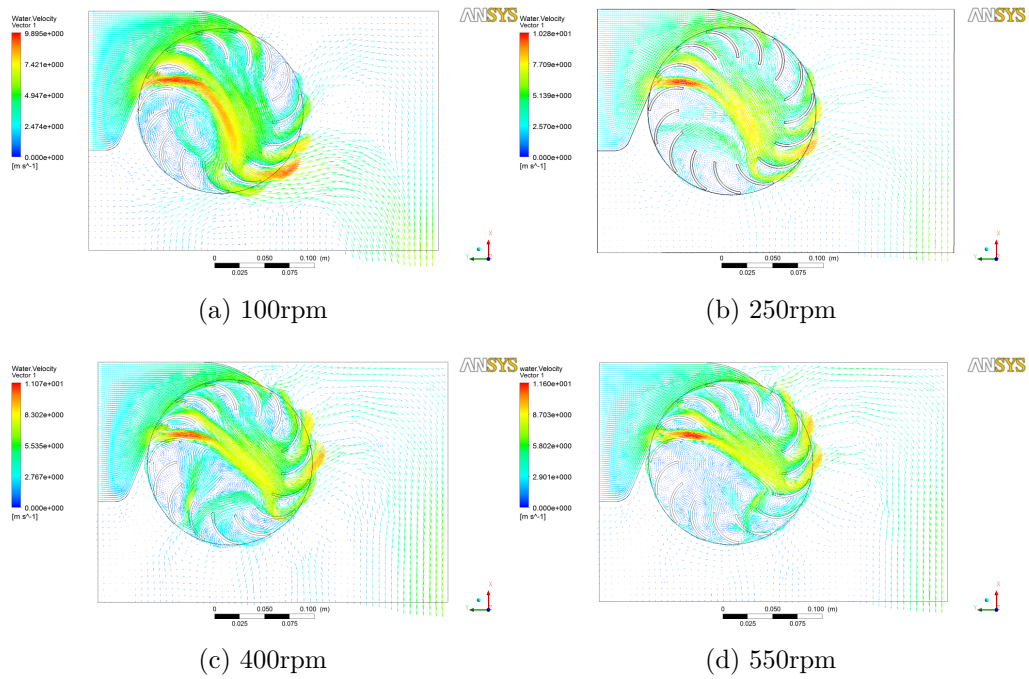
Figure 5.11: Prototype D velocity vectors variation with rotational speed
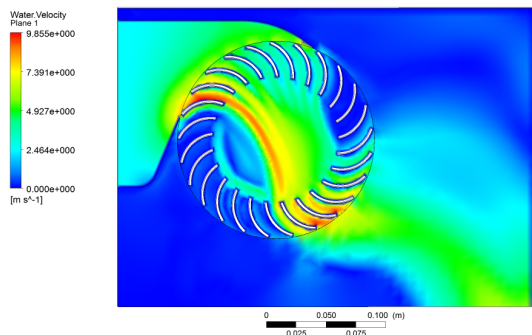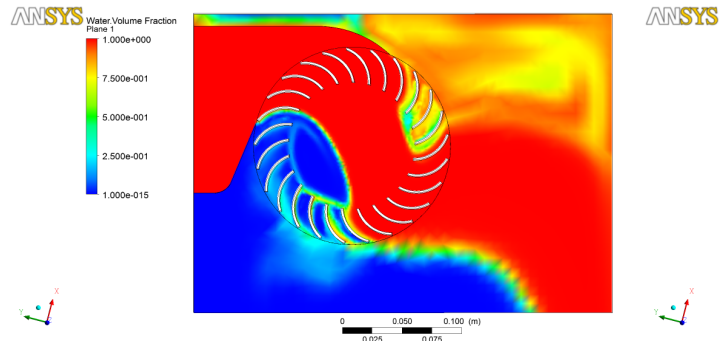
(a) water velocity at 100rpm

(b) water volume fraction at 100rpm
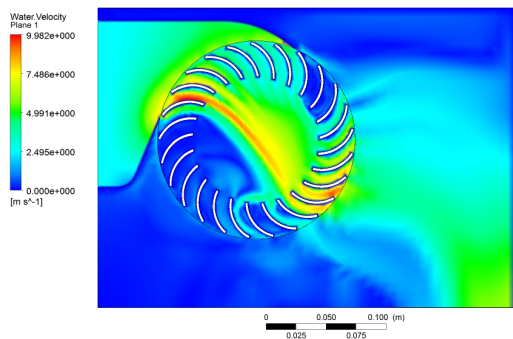
(c) water velocity at 250rpm
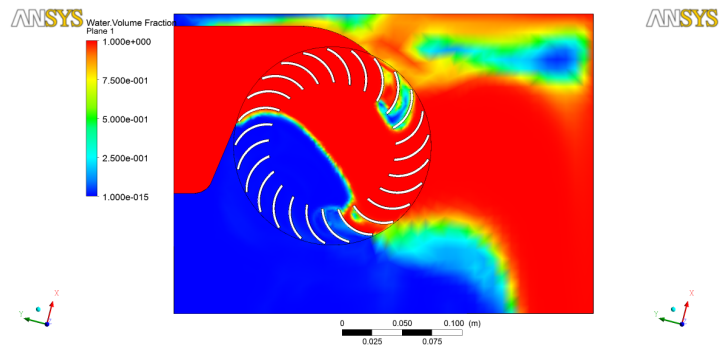
(d) water volume fraction at 250rpm
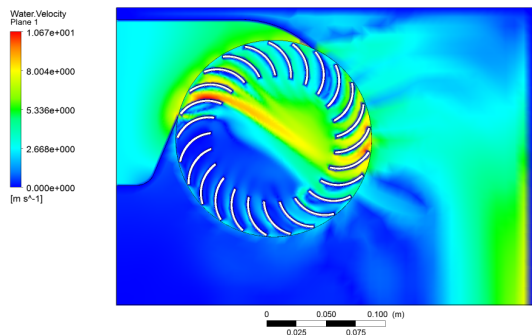
(e) water velocity at 400rpm
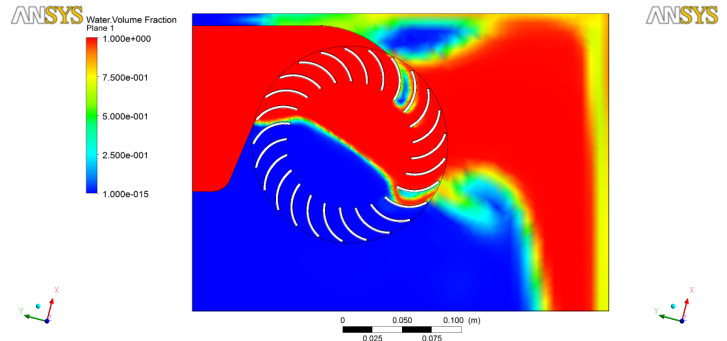
(f) water volume fraction at 400rpm
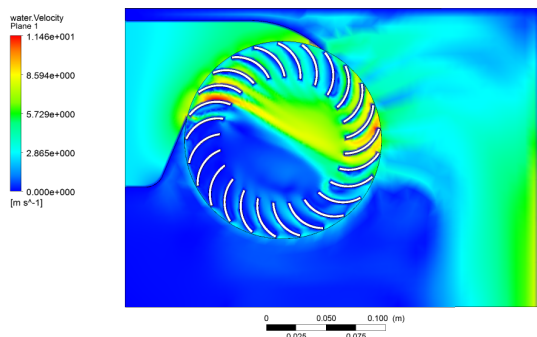
(g) water velocity at 550rpm
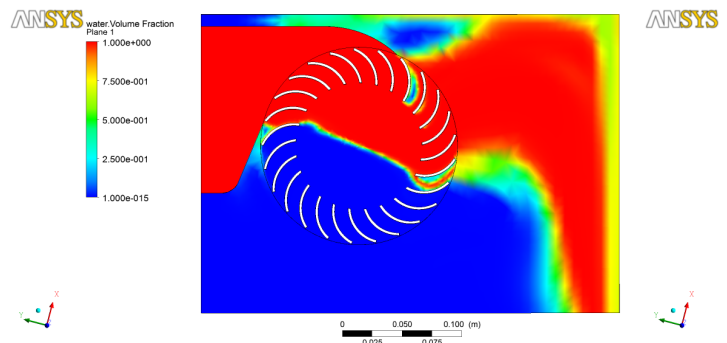
(h) water volume fraction at 550rpm

Figure 5.12: Prototype A velocity and volume fraction variation with rotational speed
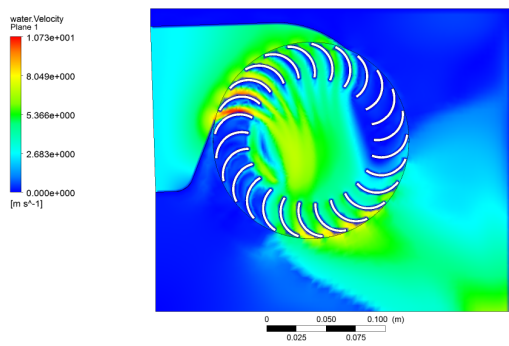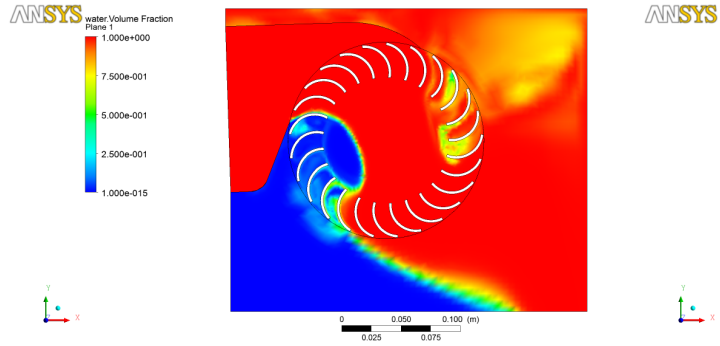
(a) water velocity at 100rpm

(b) water volume fraction at 100rpm
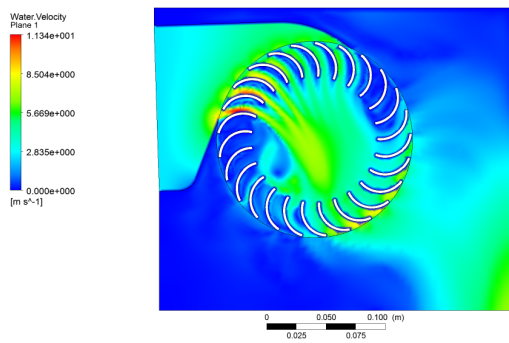
(c) water velocity at 250rpm
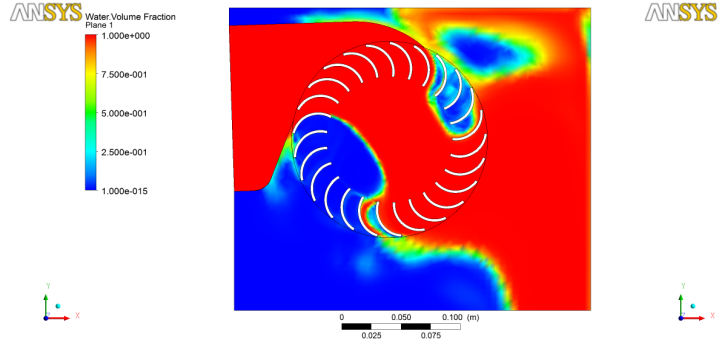
(d) water volume fraction at 250rpm
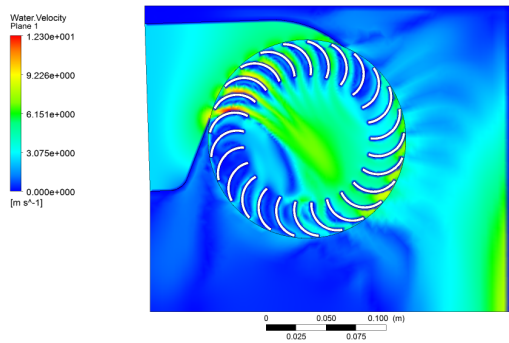
(e) water velocity at 400rpm
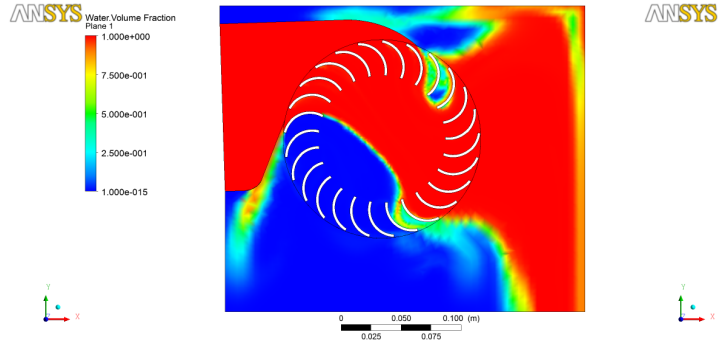
(f) water volume fraction at 400rpm
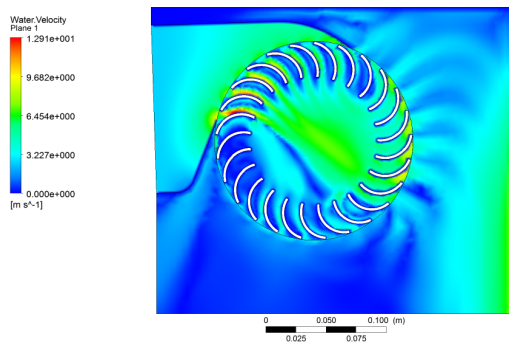
(g) water velocity at 550rpm
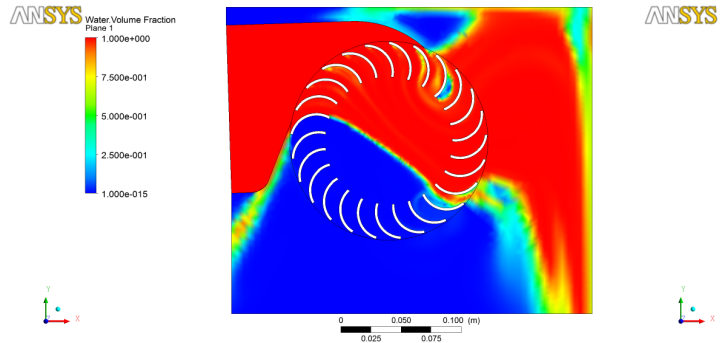
(h) water volume fraction at 550rpm

Figure 5.13: Prototype B velocity and volume fraction variation with rotational speed
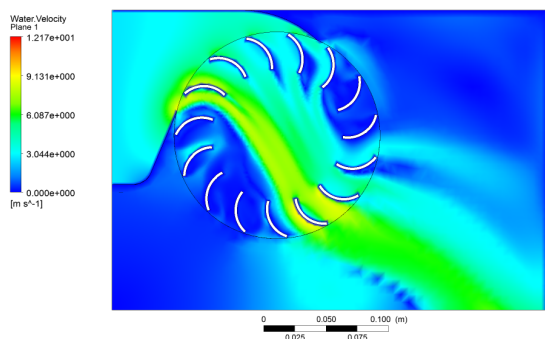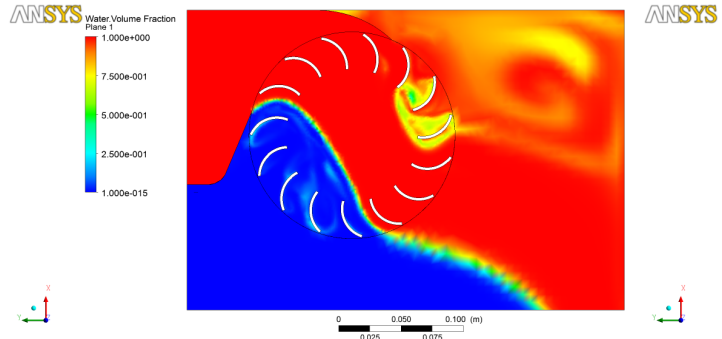
(a) water velocity at 100rpm

(b) water volume fraction at 100rpm
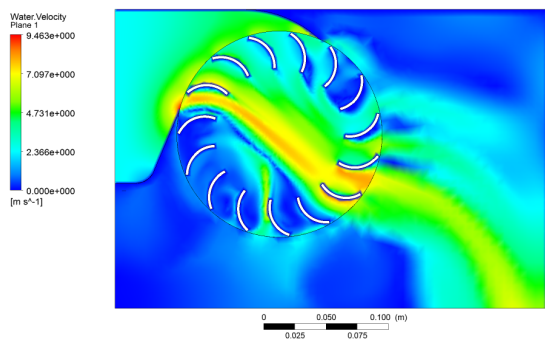
(c) water velocity at 250rpm
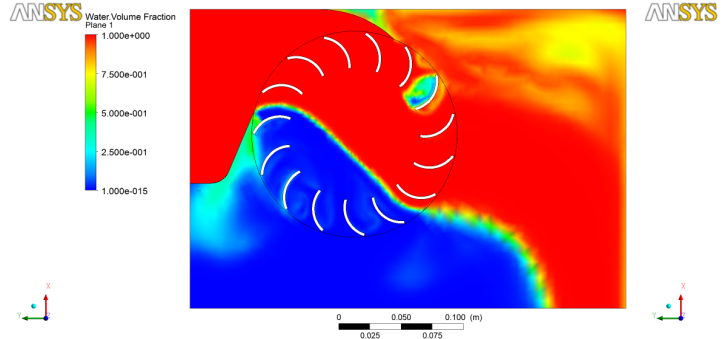
(d) water volume fraction at 250rpm
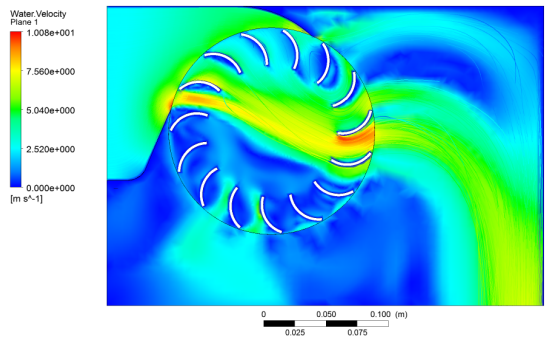
(e) water velocity at 400rpm
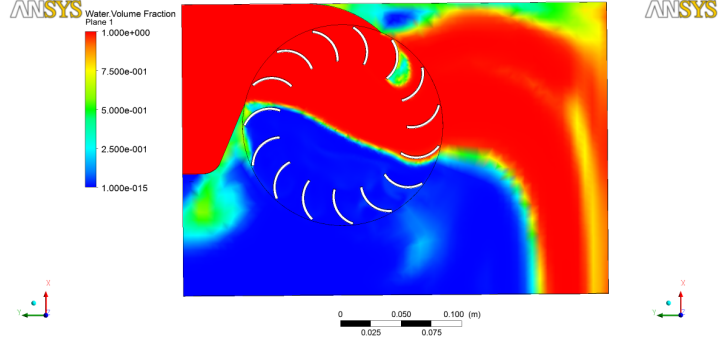
(f) water volume fraction at 400rpm
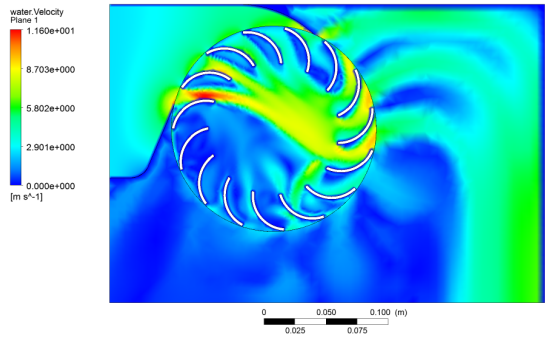
(g) water velocity at 550rpm
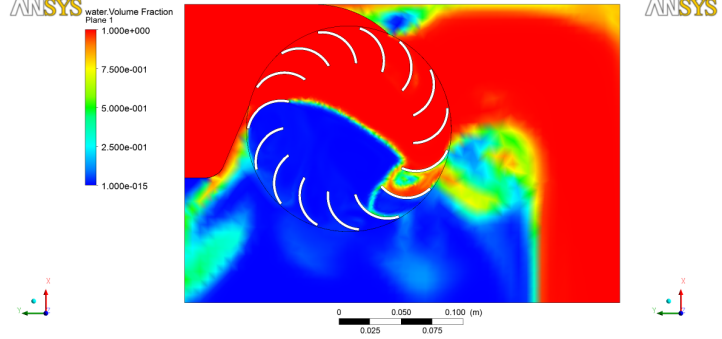
(h) water volume fraction at 550rpm

Figure 5.14: Prototype C velocity and volume fraction variation with rotational speed
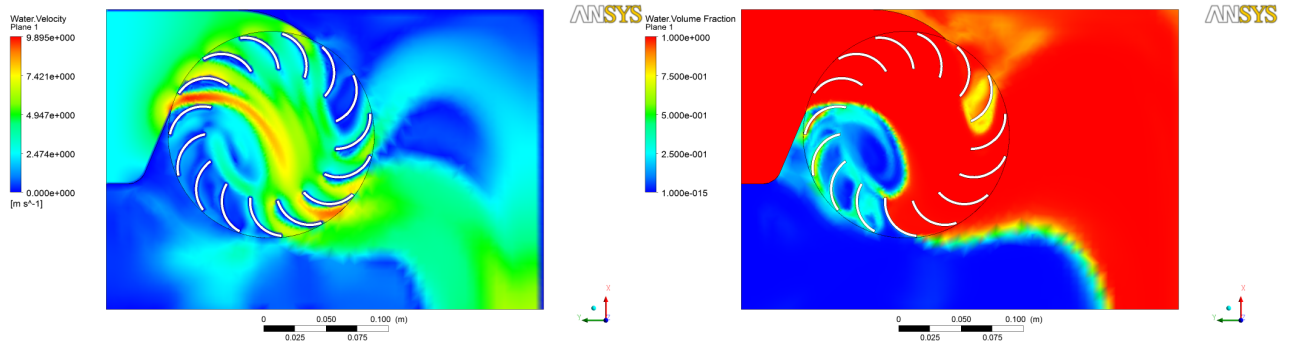
(a) water velocity at 100rpm

(b) water volume fraction at 100rpm
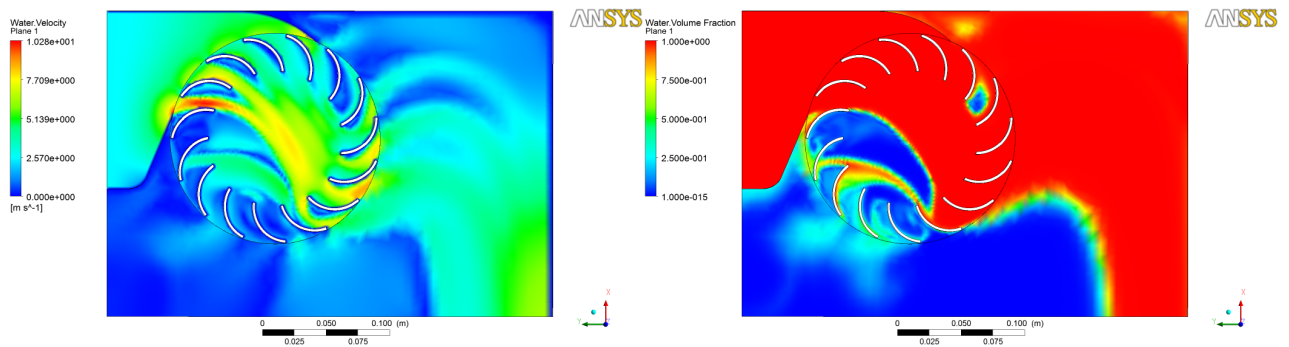
(c) water velocity at 250rpm

(d) water volume fraction at 250rpm
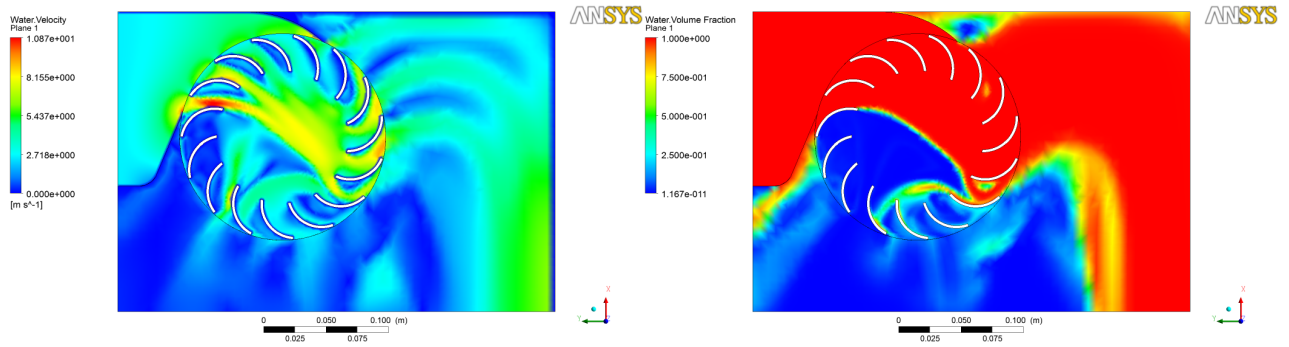
(e) water velocity at 400rpm

(f) water volume fraction at 400rpm
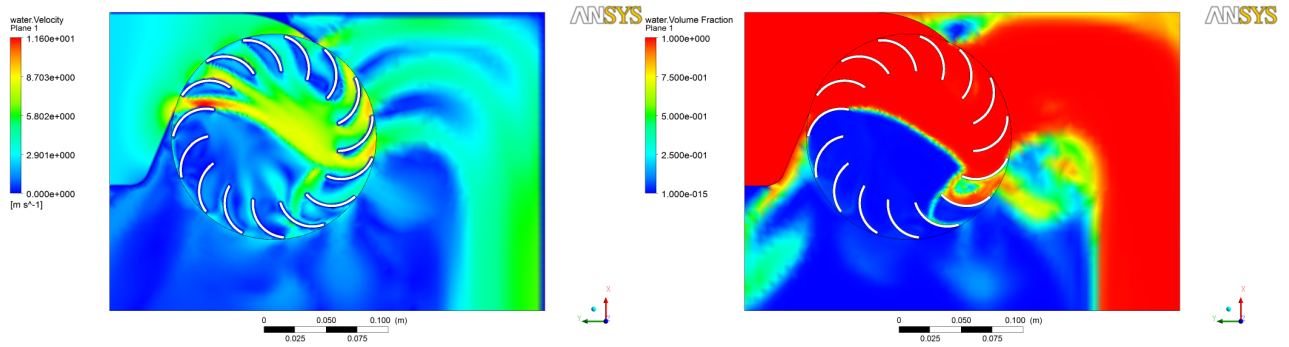
(g) water velocity at 550rpm

(h) water volume fraction at 550rpm

Figure 5.15: Prototype D velocity and volume fraction variation with rotational speed

(a) Recirculation zone

(b) Prot. A recirculation zone at 100rpm

(c) Prot. B recirculation zone at 100rpm

(d) Prot. D recirculation zone at 100rpm
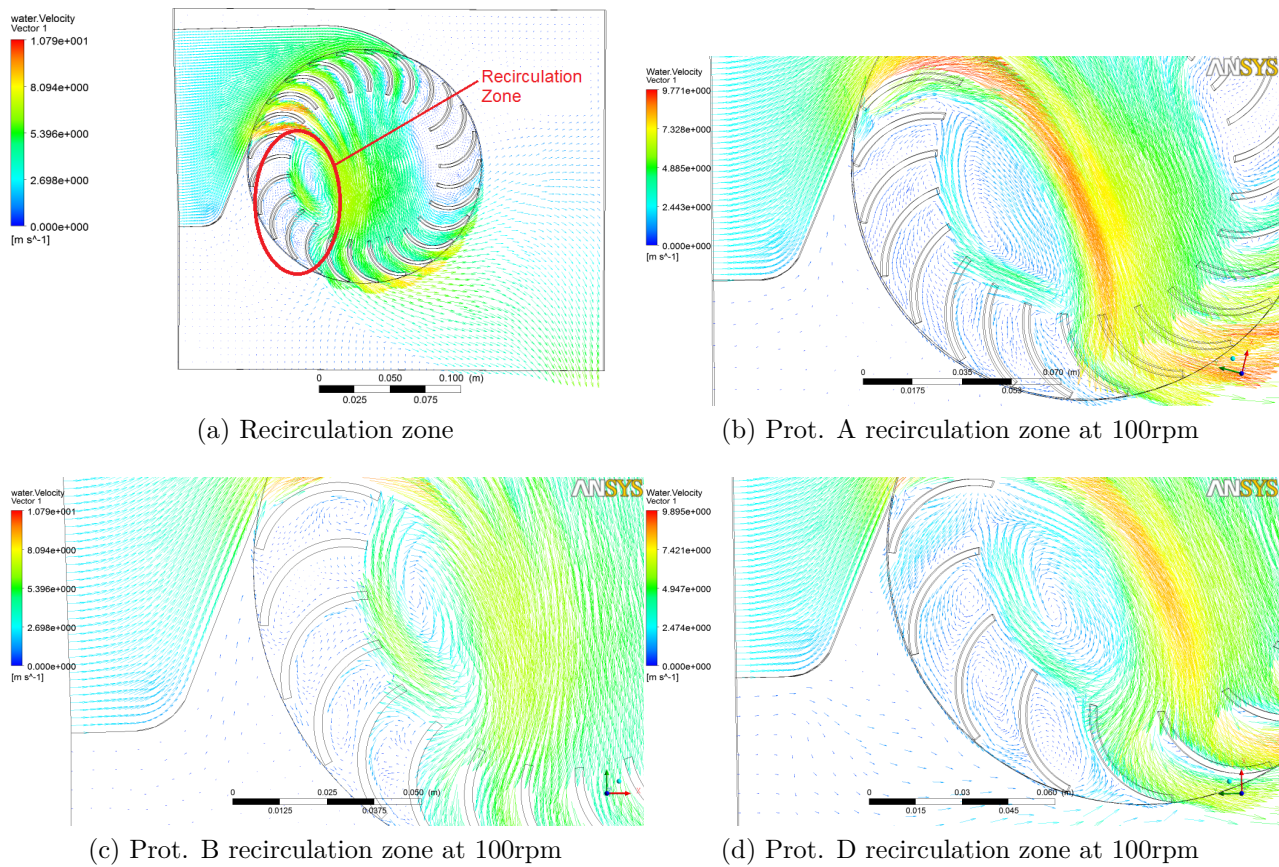
Figure 5.16: Some prototypes recirculation zone

It is very easy to notice that the fluid flow through the turbine and the water velocity are highly altered by the inlet and outlet angle of the blades, as well as by the number of blades. The water tangential velocity suffers changes in each of the two stages, becoming smaller at the outlet of first stage, on the other hand the water radial velocity component is almost the same from the first stage outlet until the water leaves the runner. The changes in the water tangential velocity component are due to the runner uses this kinetic energy for conversion into output power.

The region of recirculation is indicated in figure 5.16. According to the operation condition of rotational speed it may exists a large amount of recirculation flow, and the velocity of the recirculating flow within the blade passage is also affected by this operation condition. In some operation conditions, recirculation flow zones were detected between the blades. Additionally, the presence of a turbine casing causes a back flow of water, affecting the flow in the runner and reducing the efficiency. Another flow characteristic important to be mentioned is shown in figures 5.17 through 5.20, where the total pressure is indicated for every prototype under rotational speed variation ($100rpm$, $250rpm$, $400rpm$ and $500rpm$).

(a) 100rpm

(b) 250rpm

(c) 400rpm

(d) 550rpm
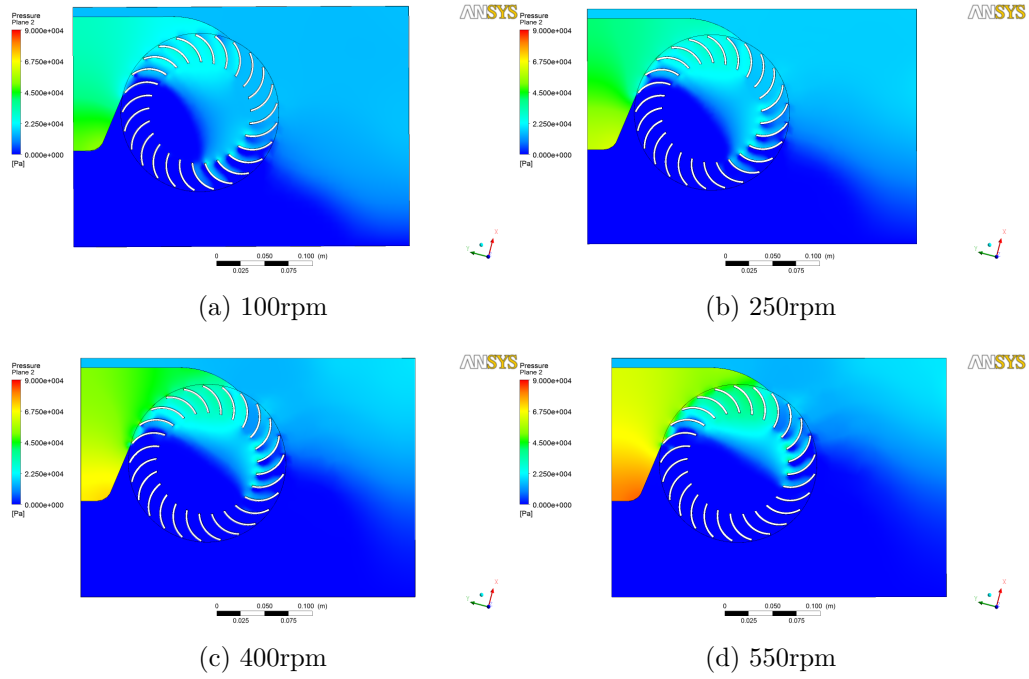
Figure 5.17: Prototype A pressure variation with rotational speed

(a) 100rpm

(b) 250rpm

(c) 400rpm

(d) 550rpm
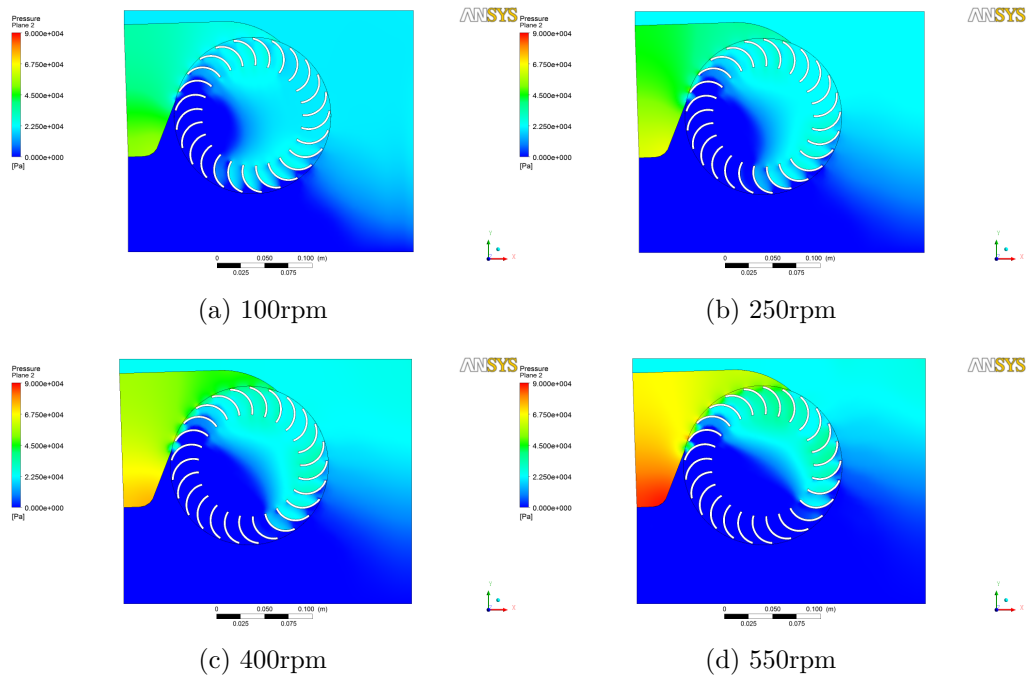
Figure 5.18: Prototype B pressure variation with rotational speed

(a) 100rpm

(b) 250rpm

(c) 400rpm

(d) 550rpm
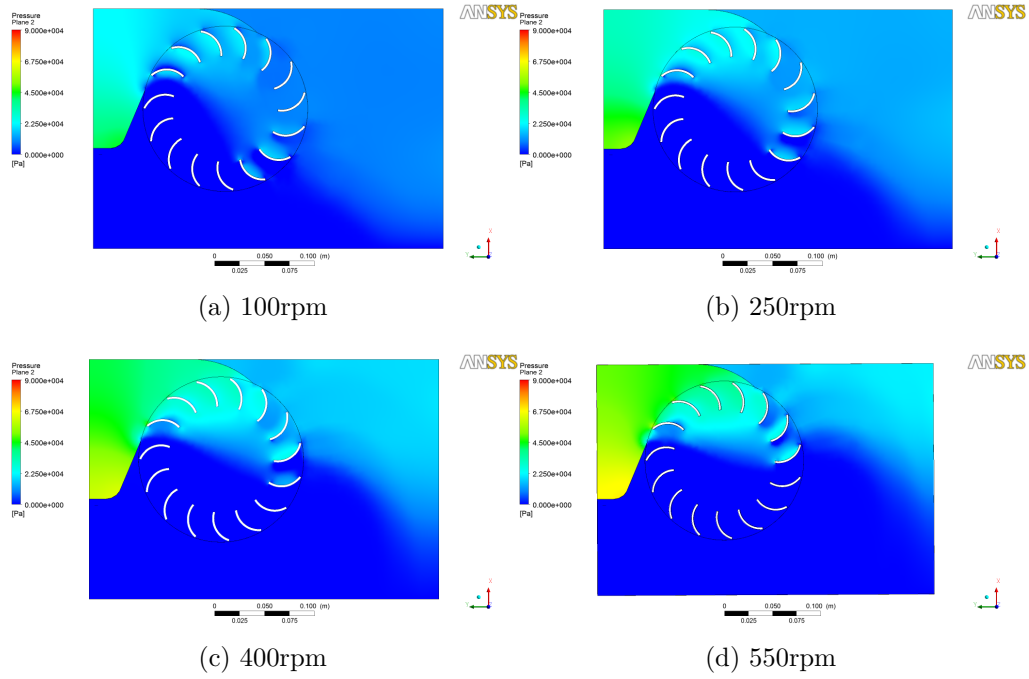
Figure 5.19: Prototype C pressure variation with rotational speed

(a) 100rpm

(b) 250rpm

(c) 400rpm

(d) 550rpm
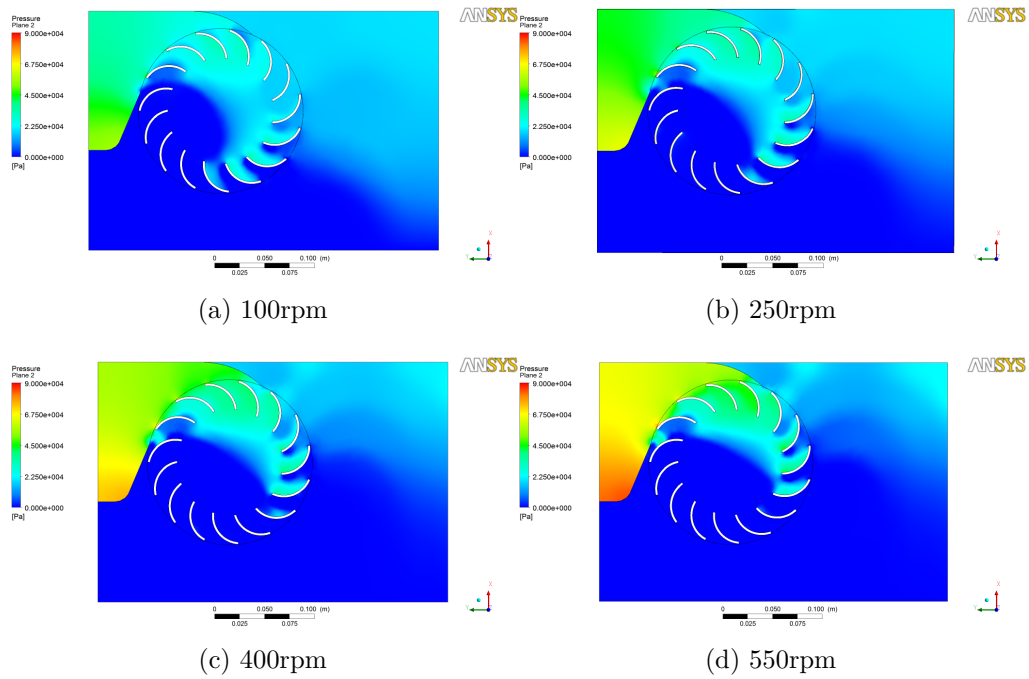
Figure 5.20: Prototype D pressure variation with rotational speed
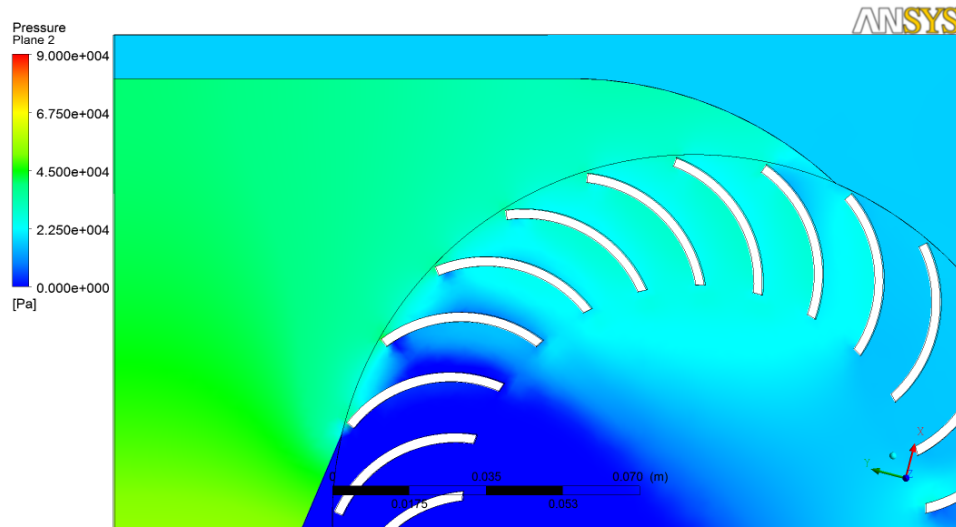
Figure 5.21: Pressure located at the nozzle outlet and runner inlet

The fluid pressure at the nozzle inlet decreases while the water flows through the nozzle and is uniformly distributed at the nozzle outlet, which is the pressure at the runner first stage. As the fluid passes through the blades at this stage, the pressure drops considerably, this can be interpreted as the conversion of the pressure in output power or kinetic energy. It is important to note that the pressure at the nozzle outlet is higher than the atmospheric as shown in figure 5.21, this behavior is consistent with the findings of Haimerl and Walseth in their studies [30, 13]. On the other hand, a very low pressure zone is detected in the recirculation region located at the lower part of the runner.

An important behavior was detected for every turbine simulated and for every rotational speed operation condition, is the entire flow that does not cross the runner and part of it remains dragged within the blades, leaving the turbine without transferring energy as shown in figure 5.22. This operating characteristic was mentioned before in the experimental studies of Walseth [13], Durgin and Fay [6]. According to the simulations, the entrained flow is more noticeable at high runner rotational speeds.

5.3.2.   Nozzle qualitative flow field analysis

In this section the results of the CFD simulations of two different nozzle configurations are presented in two subsections. The first one containing the results of the simulation of a nozzle without the inner guide vane, and the second of a nozzle with inner guide vane. Then, a short qualitative flow analysis is made. These fluid dynamic simulations were performed with a water flow rate of $Q = 13Lps$ at the nozzle inlet, the nozzle walls were set as walls with no slip
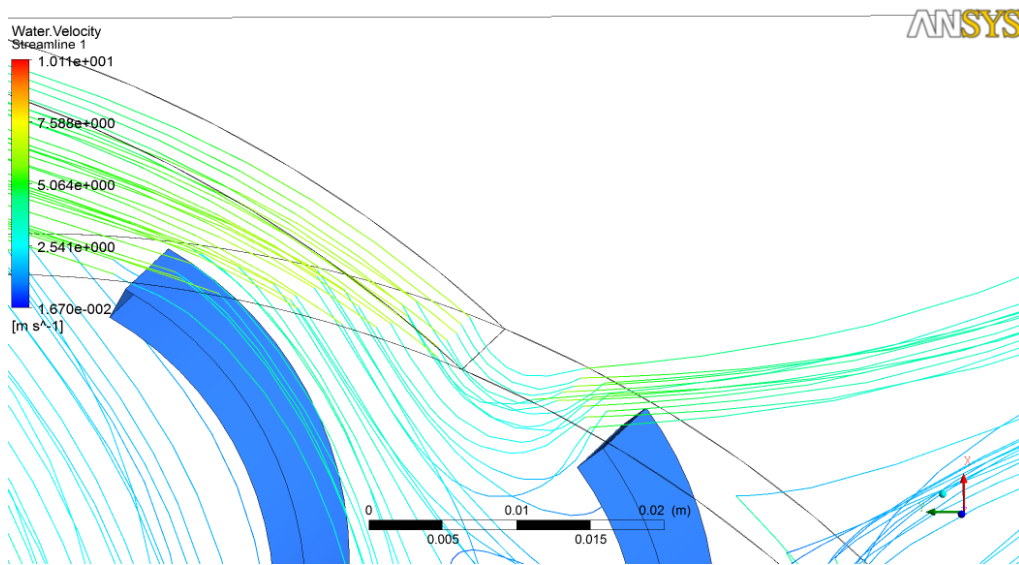
Figure 5.22: Entrained flow detected in CFD analysis

condition, at the nozzle outlet, atmospheric pressure was imposed. The results obtained show that the nozzle have a different behavior if this is coupled with the runner, for instance in the interface between these two components a pressure higher of $1atm$ is generated, as mentioned above.

Nozzle without inner guide vane

Figure 5.23 shows the pressure, velocity magnitude, velocity vectors and streamlines inside the nozzle flow field. It can be seen that the maximum pressure is obtained at the bottom of the nozzle and the minimum is located at the nozzle outlet with an uniform zero value. The water velocity at the inlet increases in its flow through the nozzle, and have its maximum value at the outlet of the nozzle. The velocity vector and streamlines figures shows a very uniform flow of water inside the nozzle.

Nozzle with inner guide vane

Figure 5.24 shows the pressure, velocity magnitude, velocity vectors and streamlines inside the nozzle with inner guide vane aligned with the water flow. It can be seen that the pressure in the nozzle with the inner guide vane increases upstream the vane, and its maximum value is located in the stagnation point, that can be found in the figure 5.24, in this nozzle configuration

the maximum velocity obtained is lower that the obtained in the nozzle without the inner guide vane, but velocity is more uniform along all the nozzle outlet.

(a) Pressure distribution

(b) Velocity

(c) Velocity vectors

(d) Streamlines
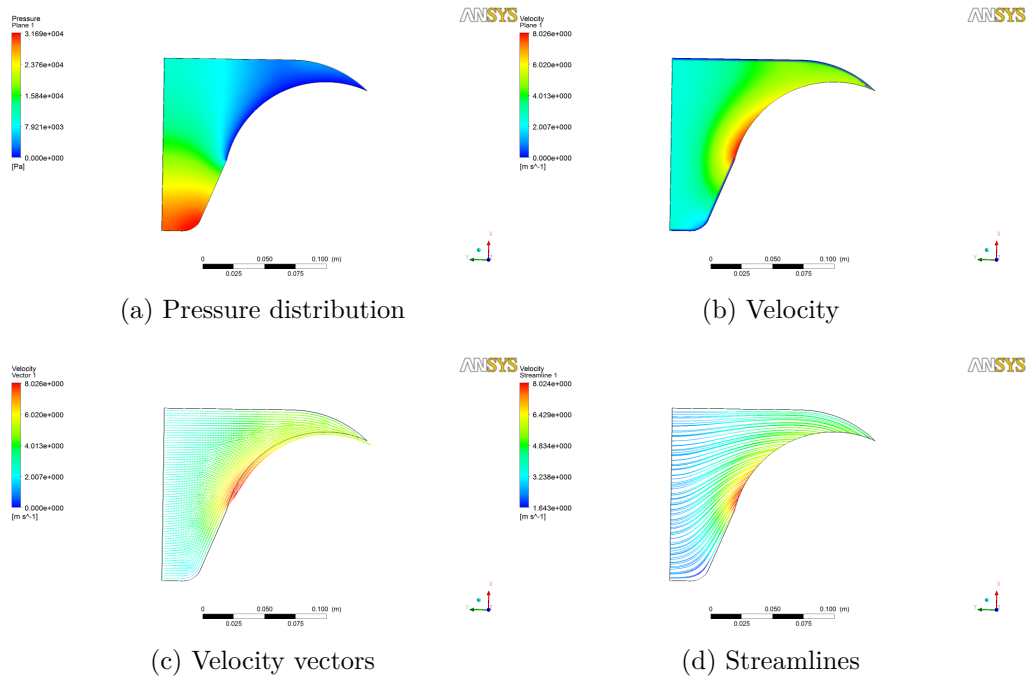
Figure 5.23: Nozzle without inner guide vane CFD results

(a) Pressure distribution

(b) Velocity


(c) Velocity vectors

(d) Streamlines
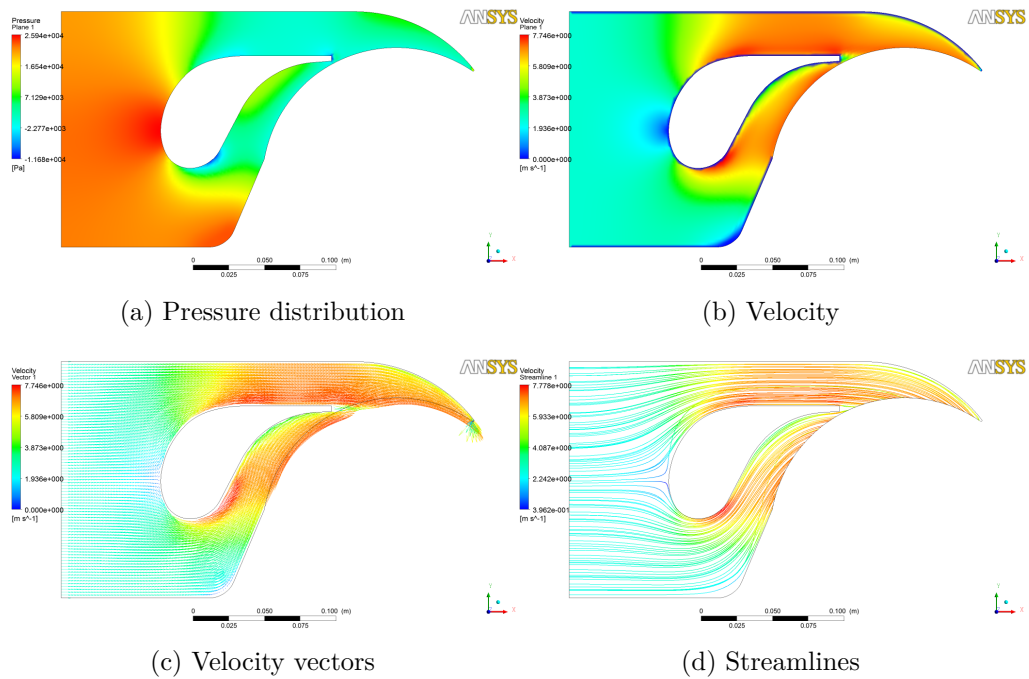
Figure 5.24: Nozzle with inner guide vane CFD results

Chapter 6

Conclusions

During the development of this project a total of four CFT prototypes were built with the necesary conditions to perform a design of experiments, every prototype had variations in runner geometrical parameters such as the blade angles and number of blades. These prototypes were tested experimentally in a test bench built for the present project. The test bench was properly instrumented and allowed to measure operating variables of the turbine as inlet water flow rate, shaft torque, runner rotational speed and inlet pressure. All of the turbine prototypes, instrumentation and the physical set up used in this project are available for using in the development of future projects in this research line.

Every prototype was tested experimentally under different operation conditions. The main objective of the tests was to collect data to calculate the efficiency and determine the performance of the prototypes. The results provided data with important information about the CFT operation. The collected data allowed to build the characteristic curves of the prototypes. From the results, it can be concluded that the prototypes with a greater number of blades were more efficient than those with less number of blades. The maximum efficiency obtained was 53.05% and the lowest was 37.80%. It can also be concluded that the best operation point for every turbine was obtained with a rotational speed value ranging from $300rpm$ to $400rpm$.

The main difference between the prototypes tested in this work and the others reported in the literature was the width of the runner. The width of all the turbines tested in the development of this project was $35mm$, this value was lower than the turbines used in most of the works actually reported. Because of this, it is likely that the effect of the runner disks walls have a greater impact in the losses of the turbines used in this work, affecting their performance.

CFD simulations of the CFT prototypes were performed reproducing similar conditions to those of the experimental tests. The obtained results gave valuable information about

the flow pattern through the turbine prototypes. The results of the simulations allowed to identify recirculation and non cross flow zones, and its behavior with the variation of the runner rotational speed. It could also be seen that the variation of the blades position has an important influence in the flow pattern, and it is presumed that this parameter had an important effect in the turbine performance, modifying the water velocity vectors. The calculation of the output power and the turbine efficiency from the CFD simulations results is of interest for further works.

From the results obtained in the design of experiments performed in this work, it is concluded that the operating conditions, as the flow rate and the runner rotational speed, influence in a major way the efficiency and the output power of the turbine. There is a positive aspect in this situation, because if the geometry can be adjusted to enhance the effects of the operational condition, an improvement in the efficiency could be obtained. Besides the importance of the operational conditions, supports the statement that this is a turbine with a simple geometry and not very high fabrication accuracies are required. Due to this the price of this turbine can be lower than other turbines, it can be a good option to be used in remote zones.

From the results it can be concluded that the cross flow turbine needs more research in order to improve its efficiency. The experiments performed during this project indicate that a wider design of experiments that takes into account the interactions between more variables may provide a valuable information, and would allow to establish stronger conclusions, another aspect of research interest is the shape of the nozzle.

References

[1] Juan Peláez. Estudio del funcionamiento y propuesta de rediseño de un prototipo de picoturbina michell-banki, 2012.

[2] Enrique Llano. Estudio del funcionamiento y propuesta de rediseño de un prototipo de picoturbina michell-banki, 2012.

[3] CAH BAZO. Manual de diseño, estandarización y fabricación de equipos para pequeñas centrales hidroeléctricas. *Quito: OLADE*, 1983.

[4] World Energy Council. World energy resources. Technical report, World Energy Council, 2013.

[5] C. A. Mockmore and F. Merryfield. The banki water turbine. *Engineering Experiment Station Bulletin Series No. 25*, 1949.

[6] WW Durgin and WK Fay. Some fluid flow characteristics of a cross-flow type hydraulic turbine. *Small Hydro Power Fluid Machinery*, pages p77–83, 1984.

[7] S. Khosrowpanah, A. A. Fiuzat, and M. L. Alberston. Experimental study of cross-flow turbine. *Journal of Hydraulic Engineering*, 1988.

[8] Abbas A Fiuzat and Bhushan P Akerkar. Power outputs of two stages of cross-flow turbine. *Journal of Energy Engineering*, 117(2):57–70, 1991.

[9] V. Seshadri C. B. Joshi and S. N. Singh. Parametric study on performance of cross-flow turbine. *Journal of Energy Engineering*, 1995.

[10] Venkappayya R. Desai and Nadim M. Aziz. An experimental investigation of cross-flow turbine efficiency. *Journal of Fluids Engineering*, 1994.

[11] Hayati Olgun. Investigation of the performance of a cross-flow turbine. *International Journal of Energy Research*, 22(11):953–964, 1998.

[12] N.H. Costa Pereira and J.E. Borges. Study of the nozzle flow in a cross-flow turbine. *International Journal of Mechanical Sciences*, 38(3):283 – 302, 1996.

[13] Eve Cathrin Walseth. *Investigation of the Flow through the Runner of a Cross-Flow Turbine*. PhD thesis, Norwegian University of Science and Technology, 2009.

[14] Junichiro FUKUTOMI, Yoshiyuki NAKASE, and Takashi Watanabe. A numerical method of free jet from a cross-flow turbine nozzle. *Bulletin of the JSME*, 28(241):1436–1440, 1985.

[15] YD Choi, J I Lim, CG Kim, YT Kim, and YH Lee. Cfd analysis for the performance of cross-flow hydraulic turbine with the variation of blade angle. In *New Trends in Fluid Mechanics Research*, pages 428–431. Springer, 2009.

[16] Young-Do Choi, Chang-Goo Kim, You-Taek Kim, and Young-Ho Lee. Determination of optimum nozzle shape of a direct drive turbine by cfd analysis. In *Fluid Machinery and Fluid Mechanics*, pages 322–327. Springer, 2009.

[17] Sung-Woo Son, Morihito Inagaki, Chang-Min Han, and Young-Do Choi. Effect of inlet nozzle shape and draft tube on the performance of cross-flow turbine for small hydropower.

[18] Young-Do. Choi, Jae-Ik. Lim, You-Taek. Kim, and Young-Ho Lee. Performance and internal flow characteristics of a cross-flow hydro turbine by the shapes of nozzle and runner blade. *Journal of Fluid Science and Technology*, 2008.

[19] Y. D. Choi, H. Y. Yoon, M. Inagaki, S. Ooike, Y. J. Kim, and Y. H. Lee. Performance improvement of a cross-flow hydro turbine by air layer effect. *25th IAHR Symposium on Hydraulic Machinery and Systems*, 2010.

[20] Ariel R Marchegiani, Norberto M Nigro, and Mario A Storti. Modelacion numerica del flujo en el inyector de una turbina hidráulica de flujo transversal. *Mecánica Computacional*, 21:683–699.

[21] S. Gonzáles Chávez and R. B Cotacallapa Vera. Modelamiento de los parámetros de funcionamiento de la turbina hidráulica de flujo cruzado aplicando el método de elementos finitos.

[22] Caner Akcan, Mahmut Faruk Akşit, Serdar Aksoy, and Ebubekir Yüksel. Response surface modeling of a small crossflow hydro turbine rotor. 2008.

[23] Jesús De Andrade, Christian Curiel, Frank Kenyery, Orlando Aguillón, Auristela Vásquez, and Miguel Asuaje. Numerical investigation of the internal flow in a banki turbine. *International Journal of Rotating Machinery*, 2011, 2011.

[24] Vincenzo Sammartano, Costanza Aricò, Armando Carravetta, Oreste Fecarotta, and Tullio Tucciarelli. Banki-michell optimal design by computational fluid dynamics testing and hydrodynamic analysis. *Energies*, 6(5):2362–2385, 2013.

[25] Hayati Olgun. Effect of interior guide tubes in cross-flow turbine runner on turbine performance. *International journal of energy research*, 24(11):953–964, 2000.

[26] Kiyoshi Kokubu, Toshiaki Kanemoto, and Keisuke Yamasaki. Guide vane with current plate to improve efficiency of cross flow turbine. *Open Journal of Fluid Dynamics*, 3:28–35, 2013.

[27] K Kokubu, K Yamasaki, H Honda, and T Kanemoto. Effect of inner guide on performances of cross flow turbine. In *IOP Conference Series: Earth and Environmental Science*, volume 15, page 042035. IOP Publishing, 2012.

[28] Kiyoshi Kokubu, Sung-Woo Son, Toshiaki Kanemoto, and Young-Do Choi. Internal flow analysis on a micro cross-flow type hydro turbine at very low specific speed range. 2011.

[29] OBAID ZIA, OSAMA ABDUL GHANI, SYED TALHA WASIF, and ZOHAIB HAMID. Design, fabrication and installation of a micro-hydro power plant. 2010.

[30] LA Haimerl. The crossflow turbine. *Water Power*, 12(1):5–13, 1960.

[31] WR Breslin. *Small Michell (Banki) Turbine: A Construction Manual.* Volunteers in Technical Assistance, 1980.

[32] A Cengel Yunus and John M Cimbala. Fluid mechanics: fundamentals and applications. *International Edition, McGraw Hill Publication*, pages 185–201, 2006.

[33] *Hydraulic Turbines and Pump-Turbines.* ASME, 2011.

[34] Humberto Gutiérrez Pulido and Ramón de la Vara Salazar. *Análisis y diseño de experimentos*, volume 2. Editorial McGraw Hill, México, 2003.

[35] Douglas C Montgomery, Douglas C Montgomery, and Douglas C Montgomery. *Design and analysis of experiments*, volume 7. Wiley New York, 1997.

[36] HK Versteeg and W Malalasekera. An introduction to cfd. the finite volume method, 1995.

[37] Yunus A Çengel and Afshin Jahanshahi Ghajar. *Heat and mass transfer: fundamentals & applications.* McGraw-Hill, 2011.

[38] Lorentz Fjellanger Barstad. *CFD Analysis of a Pelton Turbine.* PhD thesis, Norwegian University of Science and Technology, 2012.

[39] AF Mills and BH Chang. Error analysis of experiments. *UCLA, Los Angeles, CA*, 2004.

[40] CFX ANSYS. Ansys cfx. *Reference Guide. Release*, 13(0), 2010.